Rapid exhumation since at least 13 Ma in the Himalaya recorded by detrital apatite fission-track dating of Bengal fan (IODP Expedition 354) and modern Himalayan river sediments

P Huyghe, M Bernet, Albert Galy, M Naylor, J Cruz, B R Gyawali, L Gemignani, Jean-louis Mugnier

Rapid exhumation since at least 13 Ma in the Himalaya recorded by detrital apatite fission-track dating of Bengal fan (IODP Expedition 354) and modern Himalayan river sediments

P. Huyghe[a,*], M. Bernet[a], A. Galy[b], M. Naylor[c], J. Cruz[d], B.R. Gyawali[e], L. Gemignani[f], J.L. Mugnier[g]

[a]*ISTerre, Université Grenoble Alpes, CNRS, 38058 Grenoble, France*

[b]*CRPG, Université de Lorraine, 54500 Vandœuvre-Lès-Nancy, France*

[c]*University of Edinburgh, School of Geosciences, Endinburgh, UK*

[d]*Florida State University, Earth, Ocean & Atmospheric Sciences. Tallahassee, FL. USA*

[e]*Department of Physics (Geology), Central Campus of Technology Tribhuvan University, Nepal*

[f] *Department of Earth Sciences, Vrije Universiteit Amsterdam, 1081 HV Amsterdam, the Netherlands*

[g]*ISTerre, Université Savoie Mont Blanc, CNRS, 38058 Grenoble, France*

* *Corresponding author: pascale.huyghe@univ-grenoble-alpes.fr*

Keywords: Bengal fan, Himalayan rivers, Siwaliks, detrital apatite fission-track data, lag time, exhumation, erosion, threshold hillslope

Abstract

Apatite fission-track analysis of middle Bengal fan sediments (IODP expedition 354) and modern Himalayan river sediments shows that most of the detrital apatites are very young compared to their depositional ages, independent of their uranium content. Bengal fan apatites display an average central age lag time as short as 2.26±1.6 Myr since at least ~13 Ma. Such lag times reflect a mean exhumation rate on the order of at least 1-3 km/Myr. The occurrence of detrital apatites with relatively short AFT lag times since at least 13 Ma indicates that there have always been areas of rapid erosional exhumation, supplying detrital apatites to the fluvial system and delivering them to the paleo-Ganges and/or –Brahmaputra plains and finally to the Bengal fan. It also supports that temporary storage of detrital apatites in the floodplains or delta has always been negligible since at least 13 Ma. Comparison of the AFT data of the Bengal fan with those of the Central and Eastern proximal Neogene Himalayan foreland basin shows that both paleo-Ganga and –Brahmaputra catchments provided apatites with similar short lag time to the distal Bengal Fan basin.

In the modern drainage system of the Bengal fan, the apatites with young fission-track cooling ages are principally derived from areas where the topography has a sharp relief controlled by threshold hillslope processes and stream power resulting in landslide erosion as a coupled response to tectonic and fluvial forcing. By analogy with the modern erosion processes in the Himalayan range, we suggest that over the past 13 Ma, apatites were mainly derived from areas of sharp relief, where river stream power was high and hill slopes close to the threshold angle. As the exhumation signal is rather consistent since the late Miocene the detrital apatite fission-track data are either not sensitive enough to detect rapid climatically controlled changes in exhumation rates, or overall long-term erosion rates on the orogen scale are not strongly affected by climatic variations such as the variability of the Indian Summer Monsoon. Given the already rapid exhumation rates controlled by tectonics, the impact of climate

variability on surface erosion rates cannot be detected with our data, especially in the case of erosion processes dominated by threshold hillslope model.

1. Introduction

Understanding the dynamics of convergent mountain building, the sequence of thrusting and rates of erosional exhumation are crucial for understanding crustal deformation and for studying the influence of sediment flux on ocean geochemistry or tectonic and climatic coupling. The rate at which rocks are exhumed by erosion and the derived sediment transported to adjacent sedimentary basins is at the centre of studying the relationship between tectonic and surface processes in orogenic mountain belts. Given the large volume of particulate materials delivered by the Ganges and Brahmaputra rivers to the Indian Ocean at least since the Late Eocene – Oligocene (Najman et al., 2008), the study of Himalayan mountain building is of prime interest (Fig. 1A). Geological field studies provide a valuable, but partial, record of Himalayan mountain building. The mineralogical, isotopic and thermochronological analysis of Neogene sedimentary rocks provide a complementary dataset that records the unroofing history of the Himalaya, either from the proximal Siwaliks foreland basin (e.g. DeCelles et al., 2001, Huyghe et al., 2001; Bernet et al., 2006; van der Beek et al. 2006, Chirouze et al., 2013), or the Bengal fan turbidite deposits at the ODP 116 and DSDP 218 sites (e.g. Corrigan and Crowley, 1990; Copeland and Harrison, 1990; Galy et al., 1996; Galy et al., 2010).

Thermochronology of detrital grains in modern rivers or ancient sediments allows estimating present-day or paleo-exhumation rates from the lag times between the apparent cooling age and the depositional age of the detrital material in the river, the foreland basin or on the submarine fan (e.g. Cerveny et al., 1988). Using apatite fission-track (AFT) low-temperature

thermochronology, the exhumation record from the Siwalik foreland basin and modern river deposits is restricted to the period of the past ~7 Ma because post-depositional partial annealing of fission tracks in apatites affected AFT ages in deeply buried sedimentary rocks (van der Beek et al., 2006; Chirouze et al., 2013). The Bengal fan presents a thinner, more condensed, Neogene section, and therefore much less buried, which allows extending the exhumation back to the mid-Miocene (Corrigan and Crowley, 1990). Here we present AFT data of twenty-three new detrital samples from the <20 Ma record of the Bengal fan at 8°N in the Indian Ocean collected in 2015 during the IODP expedition 354 (Fig. 1A; France-Lanord et al., 2016). In addition, AFT data from six new modern river samples are also presented, together with published data from two other rivers in order to decipher the detrital record linked to the present-day Himalayan exhumation pattern (Fig. 1A).

In this paper, we show that detrital apatite with young fission-track ages and short lag times dominate the Bengal fan sediments back to at least 13 Ma, similar to the exhumation signal seen in the river sediments. This implies that fast exhumation, at least in some of the Himalayan hinterland domains existed since at least that time. By analogy with the modern system, we propose that erosion is mainly controlled by sharp relief, where river stream power was high and hill slopes close to the threshold angle. As the method that we use for the acquisition of the AFT in the Bengal Fan is similar to that used in the Siwalik foreland basin of Central and Eastern Himalaya, we compare the two exhumation records. Therefore, we suggest that source rocks from Central and Eastern Himalaya equally contributed to the AFT short lag time recorded in the Bengal Fan. Finally, we discuss the impact of climate variability on surface erosion rates.

2. Geological setting

99 *2.1. Himalayan geology*

100 The collision between the Indian and Asian plates began during late Paleocene - early
101 Eocene times along the Indus-Yarlung suture zone (IYSZ), which juxtaposes the pre-collision
102 Indian passive margin sequence to the south with the Cretaceous-Paleogene Andean-type
103 Asian Transhimalayan batholiths and ophiolites to the north (e.g. Hu et al., 2015). South of
104 the IYSZ, the Main Himalayan Thrust (MHT) accommodated convergence (e.g. Bollinger et
105 al., 2006 and references herein), generating the Himalayan structure that consists of four major
106 lithotectonic units delimited by north-dipping faults branching off the basal MHT. From north
107 to south, these faults are the South Tibetan detachment, which separates the Neoproterozoic to
108 Eocene Tethyan Sedimentary Series from the high-grade metasedimentary rocks and granites
109 of the Greater Himalayan sequence. The Main Central thrust separates the Greater Himalayan
110 sequence rocks from low-grade metasedimentary rocks of the Lesser Himalayan sequence.
111 The Lesser Himalayan thrust system places the Lesser Himalayan rocks over the Siwalik
112 Group clastic rocks of the Neogene foreland basin, which in turn were thrusted over the
113 Ganges and Brahmaputra alluvial plains along the Main Frontal thrust. East and West of the
114 Himalayan arc, the Namche Barwa and the Nanga Parbat syntaxes, respectively, constitute
115 north-south trending antiformal structures exposing high-grade metamorphic rocks of Indian
116 origin (e.g. Zeitler et al., 2001; Seward and Burg, 2008).

117 The long-term exhumation of the Himalayan range has already been recorded since
118 ~12 Ma by low-temperature thermochronometers such as zircon fission track (ZFT) or white
119 mica ^{40}Ar-^{39}Ar dating of detrital grains preserved in the Siwalik sediments of Western, Central
120 and Eastern Himalaya (e.g. Cerveny et al., 1988; Bernet et al., 2006; Szulc et al., 2006;
121 Chirouze et al., 2013). From *in situ* thermochronological data, rapid exhumation is evidenced
122 in localized areas (e.g. Blythe et al., 2007; Seward and Burg, 2008; Robert et al., 2011; Thiede
123 & Ehlers, 2013). Different tectonic processes are inferred to control exhumation: 1) 20°-30°

north dipping mid-crustal ramps affecting the rather flat MHT and localized surface uplift of the hanging wall (e.g. Bollinger et al., 2006); 2) active thickening occurs within portions of the orogenic wedge (Whipple et al., 2016) and is partly related to 3) out-of-sequence steep faults merging the basal thrust system (e.g. Hodges et al., 2004). At deeper levels, the ductile behaviour of the crust also controls zones of localized exhumation (Vannay et al., 2004). It has been suggested that a major zone of exhumation existed at the leading edge of a channel flow (e.g. Godin et al., 2006) that also involved the brittle levels located above the exhumed deep levels (4 on Fig. 1B). The viscous behaviour of the deep level favours rock motion out of the convergence direction and rapid exhumation in the Himalayan syntaxes (Zeitler et al., 2001; 5 on Fig. 1B). Slab dynamics has also been inferred to control much of the tectonic deformation of the Himalayan orogenic wedge (Mugnier and Huyghe, 2006; Webb et al., 2017).As these different tectonic interpretations are still debated, most researchers agree that localized surface uplift and exhumation processes result in physiographic sharp increases of the Himalayan relief with mean elevations above 6000 m and increasing erosion rates (Burbank et al., 2003; Hodges et al., 2004; Elliott et al., 2016). In these zones and altitudes, the kinetics of weathering and soil development are thought to be far less important than the bedrock uplift rates and erosion occurs through landsliding, which increases nonlinearly until being equal to river incision (Larsen and Montgomery, 2012) and hillslope angles approaching the threshold angle (e.g. Burbank et al., 2003).

2.2.The modern Bengal Fan catchment

The modern Ganges catchment includes the Himalayan lithotectonic units described above. The modern Brahmaputra watershed also encompasses units from the IYSZ and from the Transhimalayan batholiths. Indo-Burmese Range material and the Precambrian Indian basement of the Mikir Hills/Shillong Plateau and its Tertiary sedimentary cover may also

148 slightly contribute to the sediment load of the Brahmaputra River (Lupker et al., 2017 and
149 references therein).

150 The modern Ganges and Brahmaputra catchments provide respectively about 390±30 x
151 10^6 and 400-1160 x 10^6 tons/yr of sediment to the Bengal Fan (Lupker et al., 2017 and
152 references therein). Overall present-day erosion rates of 0.7 to 1.2 mm/yr and 1.0-1.1mm/yr on
153 the 10^3-10^4 years time scale for respectively the entire Tsangpo-Brahmaputra and Ganga
154 catchments have been deduced from ^{10}Be analyses of detrital quartz of river sands (Lupker et
155 al., 2017). Such rates may differ from long-term average exhumation rates derived from
156 detrital apatite or zircon fission track data. The Lesser and Greater Himalayan domains are
157 locally exhumed with mean rates of about 1.8 mm/yr and up to 5 mm/yr, respectively, based
158 on detrital AFT and ZFT data and *in situ* AFT (Bernet et al., 2006; van der Beek et al., 2006;
159 Blythe et al., 2007; Thiede and Ehlers, 2013 and references therein). North of the IYSZ, the
160 Transhimalayan batholiths had a very episodic history of erosion with some intervals with less
161 than 0.3 mm/year and others exceeding 4 mm/year (Copeland et al., 1987) whereas the
162 Namche Barwa syntaxis experiences exhumation at rates of up to 5-10 mm/yr (e.g. Seward
163 and Burg, 2008). Therefore the exhumation of the Himalaya varies in time and space: fast
164 exhumation rates only occur in some locations of the Himalaya (e.g. Thiede & Ehlers, 2013)
165 and are then greater than the average erosion rates.
166

167 ## 3. Sampling

168 The IODP Expedition 354 drilled the Bengal fan at 8°N (Fig. 1A). This study is based
169 on the deepest sites (U1450) and (U1451) which reached ~ 800 m and ~1200 m below sea
170 floor respectively (Table 1), recovering Quaternary to Paleogene turbidite and hemipelagic
171 sediments (France-Lanord et al., 2016). The samples consist of siltstones and fine-grained
172 sandstones, corresponding to the coarsest basal parts of thick turbidites, stratigraphically dated

by the micro- and nanno-fauna present in the intercalated hemipelagic deposits. Mineralogical and geochemical analyses showed that the turbidite material has very strong affinity to sand and silt of the modern Ganges and Brahmaputra rivers and are therefore relevant for reconstructing erosion and changes in Himalayan hinterland source areas (France-Lanord et al., 2016). For this study, we use the stratigraphic age model established by France-Lanord et al. (2016) from the mean age of the nannofossils, foraminifera and Chrons acquired onboard refined for the <1.9 Ma deposits by the magnetostratigraphic model of Reilly (2018). The uncertainty in the depositional > 1.9 Ma ages is taken as the difference between the mean age from France-Lanord et al. (2016) and the age of the youngest fauna considering that older fauna in turbidite horizons could be recycled from previously deposited sediments on the fan, resulting in a depositional age estimates that is too old.

In addition, eight modern river sand samples from the Ganges-Brahmaputra catchment have been used in this study, six new samples (Fig. 1A, Table 2), and published detrital AFT data of the Kameng and Rangit river samples were taken from Chirouze et al. (2013) and Abrahami et al. (2016) respectively.

4. Apatite Fission-Track analysis

Apatite is an accessory mineral and only represents about one in every 1000 detrital grains in the Ganges and Brahmaputra sands (Garzanti et al., 2010), but it can be readily found in river and marine sediments, and the Bengal fan turbidites (Corrigan and Crowley, 1990). Even though the fraction is small for most samples sufficient apatite crystals were recovered for fission-track dating. We used the 80-160 µm fraction of fine-grained sandstone for AFT analysis. Apatite grains were separated using standard heavy liquid and magnetic separation techniques. Apatite aliquots were mounted in epoxy, polished to expose internal crystal surfaces, and etched for 20 s at 21°C with 5.5 M HNO_3. All samples were covered with

198 muscovite mica sheets as external detectors and sent for neutron irradiation to the FRM II
199 Research Reactor at the Technische Universität München in Garching, Germany. Apatite
200 samples were irradiated together with IRMM540R dosimeter glasses (15 ppm U) and Durango
201 and Fish Canyon Tuff age standards.

202 After irradiation the mica sheets of all samples and standards were etched for 18 min at
203 21°C in 48% HF. All datable grains, including zero-track grains, within a mount were included
204 in the analysis. Grains were selected for dating primarily on their orientation parallel to the c-
205 axis and on the basis of the grain images in the mica detectors. The samples and standards
206 were counted dry at 1250x magnification, using an Olympus BX51 optical microscope and the
207 FTStage 4.04 system of Trevor Dimitru. The objective was to date up to 100 grains per
208 sample, when that was possible, depending on available sample material and grain quality.
209
210 *4.1 Track count statistics and zero-track grains*
211 The precision of AFT grain ages depends on track counting statistics. The more
212 induced and spontaneous tracks can be counted, the smaller the individual grain age
213 uncertainty becomes (Galbraith, 2005). As we used the external detector method for AFT
214 dating in this study, one needs to be aware that the formation of induced tracks recorded in the
215 mica detectors of the unknown samples, age standards and the dosimeter glasses also have
216 Poisson distributions. This is why track counts of spontaneous and induced tracks for samples,
217 standards and dosimeter glasses are taken into account for calculating age uncertainties (see
218 age and error equations in Galbraith, 2005). In our sample set from the Bengal fan and the
219 river samples a particular challenge is to deal with a large number of apatites that do not
220 contain any (zero-track grains) or only very few (<4) spontaneous fission tracks. If a grain has
221 zero, one, two or three spontaneous fission tracks it may either have a very young apparent
222 cooling age or a very low U concentration, or both. Young low U concentration grains tend to

have large age uncertainties. This can result in apparent cooling age estimates that are younger than the depositional age without being affected by partial annealing. The true but unknown and poorly constrained cooling age of such apatite grains may well be older than the age of deposition of these grains,. In order to evaluate single grain ages of such grains we not only provide the single grain ages, but also the 95% confidence intervals in which most likely the true cooling age of each single grain lies (Galbraith, 2005). The 95% confidence intervals for each grain age were calculated with the Binomfit program of M. Brandon. In addition, for all samples central and minimum ages were calculated using the RadialPlotter program of Vermeesch (2009). The central age is an estimate of an average fission-track age of a grain-age distribution, which may be heavily over-dispersed, whereas the minimum age is an estimate of the youngest coherent grain-age population within a detrital grain-age distribution (Galbraith, 2005).

Given the relatively low closure temperature of the AFT thermochronometer (~110°C for F-OH apatite (e.g. Reiners and Brandon, 2006), and the ~60-110°C AFT partial annealing zone (PAZ) temperature range, depending on mineral chemistry and holding time within the PAZ, existing fission tracks may be progressively annealed after deposition (e.g. Reiners and Brandon, 2006). In the case of the Bengal fan most apatites are F-rich, a result already obtained by Corrigan and Crowley (1990).

4. 2 Exhumation rate estimations

As the main objective of this study was to estimate rates of exhumation from the detrital AFT data, we decided to use the minimum age approach (Galbraith, 2005 and references herein), instead of the more commonly used binomial peak-fitting approach, which was applied in previous studies on the Siwaliks Formation (van der Beek et al. 2006; Chirouze et al., 2013). For most samples this does not make a big difference, as in many cases the

248 minimum age and the first peak determined by binomial peak-fitting are identical or do
249 overlap at the 95% confidence level. Nonetheless, applying the minimum age model avoids
250 sample size (number of grains) bias to younger ages (Galbraith, 2005). Therefore, for the
251 samples that fail the χ^2 homogeneity test and that have a considerable (>20%) dispersion of
252 their single grain age distribution, the minimum age provides a more reliable estimate of the
253 first coherent age population (Galbraith, 2005). The minimum age lag time can provide an
254 estimate on the fastest exhumation rates in the source area, with the lag time being defined as
255 the difference between the apparent AFT age and the depositional age (e.g. Bernet et al.,
256 2006). The same calculation can be done with the central ages for an estimate on mean
257 exhumation rates. In the absence of post-depositional partial annealing, the lag time integrates
258 the time between cooling of the apatite below the fission-track closure temperature in the
259 source rock, exhumation towards the surface, erosion, sediment transport in the fluvial system,
260 and deposition in the Bengal fan. For the Himalaya, transport times can be considered as being
261 negligible (Lupker et al., 2017), and the lag time is considered as a direct measurement of
262 erosional and tectonic exhumation within the source area at the time of deposition. We use a
263 1D thermal advection model (Appendix D) to obtain first-order estimates of average
264 exhumation rates from our AFT lag-time data.
265
266 **5. Apatite fission-track results**
267 *5.1. Bengal fan turbidites*
268 Twenty-three samples from 17.7 to 1153.4 m below sea floor and respectively from 0.3 to 17.2
269 Ma stratigraphic age were analysed (Table 1). The results show the typical wide range of non-
270 reset detrital grain ages between 0.2 Ma and about 70 Ma with central ages ranging between
271 0.9 and 14 Ma and minimum ages between 1.7 and 12.1 Ma (Fig. 2). Most of the samples fail
272 the χ^2 test and show large grain age dispersions of >30% (see Appendix B for the details of

273 every samples). For the four samples that do pass the χ^2 test only 30 or less grains could be
274 dated. A total of nineteen samples have central ages equal or older than the depositional age at
275 the 95% confidence level. Central and minimum AFT ages are also regularly older in deeper
276 and stratigraphically older sediments (Fig. 2). For the site U1450, one sample displays both
277 central and minimum ages younger than the modelled age of deposition. For the deeper site
278 U1451, eight samples have their central and minimum ages younger than their deposition ages,
279 of which six samples are within their 2-sigma error range overlapping with the depositional
280 age (Table 1). The peculiar results of these samples are discussed below. For both sites U1450
281 and U1451, the difference between the central and the minimum ages of the Bengal fan
282 samples is on average less than 1.5 Myr and for many samples both age estimates overlap at
283 the 95% confidence level.
284 Radial plots and cumulative grain age plots with the single grain 95% age confidence intervals
285 have been performed (Figs. 3 and 4 and Appendix B). Finally, the age-U concentration
286 relationship indicates that many of the grains with <2 Ma apparent AFT cooling ages have U
287 concentrations in the 10-100 ppm U range (Fig. 5).
288
289 *5.2. Himalayan modern river sand apatite fission-track data*
290 New AFT ages of river sediments of the Brahmaputra, Siang, Sun Kosi, Daraundi Khola,
291 Marsyandi, and Bothe Kosi rivers are shown in Table 2. Grain ages of the Himalayan river
292 sands range between 0.2 Ma and about 48 Ma. The older, Eocene ages are found in the Siang
293 and Marsyandi rivers only. All the eight Himalayan river samples fail the χ^2 test (Appendix
294 C). Central ages of the Himalayan river sand samples vary between 1.2±0.2 Ma and 4.6±0.5
295 and minimum ages range between 0.66±0.66 (Rangit River) to 3.7±1 Ma (Fig. 6 and Appendix
296 B).
297

6. Discussion

Young AFT cooling ages are widely documented from *in situ* bedrock studies (e.g. Blythe et al., 2007; Thiede and Ehlers, 2013), which reinforce our findings. Below, we first detail and comment on the samples for which have AFT ages younger than the depositional ages (Table 1). We then give the implications of young AFT and short lag time ages for the long-term exhumation rates in the Ganga-Brahmaputra catchment, for the erosion processes providing young detrital apatites to the drainage system and finally its implications regarding tectonic/erosion/climate interactions over the last 13 Ma.

6.1 Interpreting apatite fission-track ages based on low track counts

The AFT age versus U concentration plot of the Bengal fan sediments shows that AFT cooling ages of <2 Ma are not restricted to grains with very low (<10 ppm) U concentrations. The same observation may be done from the detrital apatites carried by the modern Himalayan rivers (Fig. 5). Nonetheless, the interpretation of AFT ages based on low (<4) spontaneous tracks per grain, is difficult.

One could first argue that the low spontaneous track counts of the samples with younger AFT ages than their depositional age is related to post-depositional partial annealing because of reheating caused by burial heating and/or hydrothermal fluid flow. Given that 1) the sediments were collected from <1200 m below seafloor, and 2) the maximum depositional age is ~16 Ma (Fig. 2), partial annealing of fission-tracks in apatite would be highly unlikely if the basin geothermal gradient is not in excess of ~100°C/km. Present-day thermal gradients measured during IODP Expedition 354 are on the order of 40°C/km (France-Lanord et al., 2016), consistent with ocean basins of same age of 90–100 Ma and other values measured in the Bay of Bengal (Hasterok et al., 2011). For such a geothermal gradient, the 60-100°C AFT partial annealing zone is reached from burying depth of 1500 m, which is not the case for the

concerned samples (Table 1 and Fig. 2). In addition, the occurrence of smectite and the absence of illite rich smectite-illite mixed-layered clay minerals within the clay mineral fraction of the turbidites sampled for AFT analysis (France-Lanord et al., 2016), independently suggests that temperatures of partial annealing were never reached. Smectite starts to turn into illite at temperatures of 70-95°C (Lanson, 1995), which corresponds to the upper part of the AFT partial annealing zone (e.g. Reiners and Brandon, 2006). Therefore we have to consider another explanation for their young AFT ages.

Samples with only few apatite (<30 grains) may present central or minimum ages younger than the depositional age (table 1). Sample U1450A 110F is an example for this situation (Fig. 3) and only 26 single grain could be analysed with 19 grains with zero spontaneous tracks, and 6 with only 1 or 2 spontaneous tracks, leaving only 1 grain with >2 spontaneous tracks (Appendix B). An additional interesting observation is that the minimum age of this sample is older than the central age, being drawn up by the one older grain, with the highest U concentration (Fig. 3). The central and minimum ages of this sample have relatively large uncertainties. Less than 30 grains were also analysed for samples U1451A 74F4 and U1451B 51R2 generating AFT age uncertainties greater than those for samples with more grains counted (Fig. 3). Therefore, we do not consider those samples in the following.

At site U1451, more samples with minimum and/or central ages younger than the depositional age (negative lag times) can be observed especially for the deepest samples (Fig. 2 and Table 1). Sample U1451A 37F2, has central and minimum ages younger than the depositional age of 6.53±0.3 Ma. For this sample 74 grains were dated, but 32 of these grains (43%) have very low (<4) spontaneous track counts (see Appendix B), which skew the minimum and central ages to younger values, as grains with higher track counts of this sample result in ages older that the depositional age (Fig. 4). Therefore, we will not consider this sample in the following discussion and exclude these results in respect of our interpretation.

348 Samples U1451A 86F2, U1451B16 R1, U1451B 27R1, U1451B 37R2 and U1451B 45R1 all
349 have minimum or central AFT ages that overlap with the 2-sigma error range with their
350 depositional ages (Table 1). Sample U1451A 86F2 has ~20% of the 70 grains dated with <4
351 spontaneous tracks, sample U1451B 16R1 42% of 100 dated grains, sample U1451B 27R1
352 19% of 69 grains dated, sample U1451B 37R2 46% of 59 grains dated and sample U1451B
353 45R1 68% of 89 grains (Appendix B). The radial plot of U1451B 45R1 shows that higher U-
354 concentration grains have younger apparent cooling ages (Fig. 4C). The lowermost sample
355 U1451B 58R2W with a depositional age of 17.2±0.5 Ma and a 1046.89 m burial depth, has
356 minimum and central ages that are considerably younger than the depositional age (e.g.
357 negative minimum age lag times of 8.2±5.1 Myr), as shown in Table 1. For this sample only
358 32 grains could be dated of which 38% have low spontaneous track counts.
359
360 One can also note that from 550m in the U1451 site (Fig. 2), turbidite main granulometry is
361 finer and composed of clayey silt instead of fine sands in the upper stratigraphic levels and in
362 site U1450, making the sampling of apatite grain more difficult and less abundant. Therefore,
363 the stratigraphically lowermost samples just show the importance of obtaining as many single
364 grain ages as possible from high track density grains if available to get more tightly
365 constrained age estimates.
366 Our analysis underlines that the AFT dating method reaches its detection limits when dealing
367 with grains that have low spontaneous track counts and low U concentrations.

368 *6. 2. Detrital Apatite fission-track signal and modern erosion in Himalaya*

369 The average AFT central age value is 2.53±0.28 Ma and 2.9 ±0.39 for the rivers draining
370 respectively the Central and Eastern Himalaya, which are the rivers belonging to the Ganga or
371 Brahmaputra catchment (Fig. 7). The river sediments, which were obviously collected much
372 closer to their source areas than the Bengal fan sediments, provide a faithful representation of

373 the *in situ* bedrock AFT age distribution in the source (e.g. Thiede and Ehlers, 2013 and
374 references therein), suggesting a very short transit and delivery time from the source to the
375 sink. Such a short transit time is also reflected by the late Quaternary Bengal Fan AFT
376 samples, the AFT central ages of which are very similar to the Himalayan rivers AFT ages
377 discussed above (Table 2, Figs. 5-7) and suggests almost no transient storage in both the
378 fluvial plain and delta.

379 Young *in situ* AFT ages (Burbank et al., 2003; Blythe et al., 2007; Whipple et al.,
380 2016) are either found in zones close to and north of the sharp topographic transition (Fig. 1B)
381 of the Greater Himalaya domain (Thiede and Ehlers, 2013 and references therein), or in the
382 Namche Barwa and Nanga Parbat syntaxial antiforms (e.g. Zeitler et al., 2001; Seward and
383 Burg, 2008). Although the exhumed areas are narrow, laterally discontinuous, and located on
384 the southern side of the Himalaya, they provide the youngest apatite to the river system
385 (Thiede and Ehlers and references therein). Seven out of eight rivers have central ages of 3 Ma
386 or less (Table 2 and Fig. 7), for the rivers draining the sharp topographic transition and higher
387 Himalayan relief. Therefore the influence of these areas is significant with respect to sediment
388 input to the rivers. The dominance of apatite with about 2-3 Ma fission-track ages is enhanced
389 because the formations north of the sharp topographic transition mainly consist of the apatite-
390 richer Greater Himalayan Sequence (Robert et al., 2011). Focused exhumation of the steep
391 Namche Barwa syntaxis, with young AFT cooling ages (0.7-1.1 Ma *in situ* AFT ages; Seward
392 and Burg, 2008), is also significantly contributing to the Brahmaputra River (AFT minimum
393 and central ages of respectively 2.61±0.83 Ma and 3.05±0.39 Ma) close to its confluence with
394 the Ganges River.

395 The detrital AFT age value for the rivers are averaging different source areas, and the
396 small average difference for rivers draining the Central and Eastern Himalaya strongly suggest
397 a near impossibility to distinguish the provenance (Central or Eastern Himalaya) of detrital

apatite in the Bengal fan sediments (Fig. 7). Additional information, which would allow distinguishing different source rocks, would be needed. Nonetheless, in both cases, the apatites originate from areas with steep slopes of sharp relief, which are exhumed rapidly.

Exhumation rates are significantly correlated with high stream power and landslide erosion rates along steep slopes in the Namche Barwa massif (Larsen and Montgomery, 2012). Similarly, the high exhumation rates evidenced in central Himalaya by younger than 2 Ma *in situ* AFT ages (e.g. Robert et al., 2011) correlates with a sharp topographic relief displaying steep slopes close to a ~33° threshold angle (Hodges et al., 2004) and strongly incised by river channels with a high stream power (Lavé and Avouac, 2001). Almost ~14 000 landslides induced by the 2015 Gorkha earthquake are located close and to the north of this physiographic transition between Higher and Lesser Himalaya domains and are characterized by slopes greater than 35° (e.g. Tsou et al., 2018). Therefore the exhumation of the youngest detrital AFT population found downward of these zones is controlled by a threshold hillslope-model of erosion, where landscape evolution is linked to landslide erosion, tectonic uplift, fluvial forcing and efficient sediment evacuation.

6.3. Long-term exhumation signal from apatite fission-track data

The main observation drawn from the Bengal fan AFT data in this study is the occurrence of apatite with central AFT ages having lag times averaging 2.26±1.6 Myr) since the mid-Miocene (Table 1, Fig 7). These short lag times imply that some Himalayan source areas were rapidly exhumed at least at rates of 1 to 3 mm/yr, as estimated from a 1D thermal advection model for fluor apatite (Appendix D).

Previous studies in the proximal Siwalik foreland basin deposits of the Central Himalaya (van der Beek et al. 2006), and Eastern Himalaya (Coutand et al., 2016 and Chirouze et al., 2013) indicate AFT data ages that mainly range from 0.3 to 35 Ma. The

422 Bengal Fan and Siwalik data were acquired with a similar method. We compare below the
423 central AFT ages already published in the Siwaliks with the Bengal Fan AFT central ages (as
424 central and minimum ages overlap at 95% confidence level). For the last 6-7 Ma (older AFT
425 data in the Siwaliks are subjected to partial annealing), the mean lag time for the Central and
426 Eastern Siwaliks are respectively 2.47±1.7 Myr and 2.13±1.44 Myr while it is of 2.19±1.6 Myr
427 from the Bengal Fan turbidites. These results are therefore very similar and overlap at 2σ
428 level, although the catchment basin of the Bengal Fan is much greater and may contain older
429 sources than the ones of the Central and Eastern Siwalik domains (Fig. 7 and Tables 3 and 5).
430 This suggests that sources have been rapidly exhumed in both central and eastern catchments
431 from 6-7 Ma. Provenance analysis of the apatite should provide the litho-tectonic localisation
432 of young apatite and how the exhumation varies in space and time, but this is not beyond the
433 scope of this study. The lack of post depositional partial annealing for the Bengal Fan AFT
434 data allows extending the record of exhumation back to 13 Ma. It shows that for the period 7-
435 13 Ma, young apatite were also provided by the main Himalayan rivers, indicating that there
436 has always been areas of rapid erosional exhumation, supplying detrital apatites to the fluvial
437 system and delivering them to the paleo Ganges and/or Brahmaputra plains and finally to the
438 Bengal Fan. The rate of such a rapid exhumation might not correspond to the same areas
439 through time, but is relatively constant over the last 13 Ma. Another feature rising from this
440 analysis is that the Siwalik foreland basin has been an overfilled basin since at least 13 Ma.
441 Finally, the detrital apatite fission-track ages of the Bengal Fan turbidites display similar lag
442 time characteristics to the AFT ages carried by present-day Himalayan rivers. Therefore, the
443 processes described in the above section for the modern erosion in the Himalayan range could
444 be extended in the past and we suggest that, over the last 13 Ma, apatite were mainly derived
445 from areas of sharp relief, where river stream power was high and hill slopes close to the
446 threshold angle.

447

448 *6.4. Detrital fission tracks and tectonic/erosion/climate interactions over the past 13 Ma*

449 It has been suggested that erosion of the Himalaya is enhanced by the intense monsoonal
450 rainfall (e.g. Burbank et al., 2003) and that an east-west climatic gradient involving higher
451 amount of precipitation and higher erosion in the east than in the west (e.g. Bookhagen and
452 Burbank, 2010) controls the tectonics of the thrust wedge (e.g. Chalaron et al., 1995). Neither
453 an east/west regional or a temporal evolution of the exhumation is visible in the detrital AFT
454 data of the modern Himalayan rivers, in the Bengal fan deposits or in the Neogene Siwaliks
455 foreland basin deposits of the central and eastern Himalaya (Fig. 7).

456 Marked differences in precipitation and seasonality occurred within the Bengal
457 fan catchment over the past 13 Ma as suggested by stable carbon and oxygen isotopic studies
458 (e.g. Dettman et al., 2001), and they might have modified the erosion of the Himalaya and be
459 recorded in the sedimentary flux of the Bengal Fan (Krishna et al., 2016). Although these
460 climate/erosion relationships remain an active debate for the global Plio-Pleistocene (e.g.
461 Herman et al., 2013; Schildgen et al., 2018 and references therein) or for the late Miocene (e.g.
462 Clift et al., 2008), the erosion of the Himalaya has increased at the onset of the Plio-
463 Pleistocene Northern Hemisphere cooling (Herman et al., 2013) or in the Late Miocene
464 affected by an intensification of monsoon (e.g. Clift et al., 2008). Although the sedimentary
465 flux from the 12 Ma long stable drainage system (Galy et al., 2010) seems to reflect these
466 events (Krishna et al., 2016), the AFT data (Fig. 7) do not reveal any significant variation in
467 erosion rate. We suggest that this difference is linked to a mixing of material coming from
468 different domains affected by different erosion rate. In this study the minimum ages of the
469 AFT reflect the domains of the most rapid exhumation. The absence of a climatic signal in
470 these data agrees with the predictions of the threshold hillslope model (e.g. Larsen and
471 Montgomery, 2012), which is less sensitive to climatic variations, as rainfall only affects

erosion through variations of the river profiles (e.g. Whipple and Tucker, 2002), which are buffered by variations of the stream power due to changes in the river width (e.g. Lague, 2013).

Therefore the detrital AFT data do not have the precision to trace the effect of climate-variability on exhumation rates on the <2 Myr timescale. In contrast, the persistence of detrital apatite with short AFT lag times in the Bengal fan sediments may be rather linked to the distribution of tectonically driven uplift on linger time-scales, and the morphology of the mountain belt. Given that exhumation within the main Himalayan orogen since at least 13 Ma propagated southward (Fig. 8) as suggested by A) the classical forward propagating thrust systems model of e.g. DeCelles et al., (2001 or Bollinger et al., (2006); and B) the εNd studies performed in the Siwaliks of the Central Himalaya (e.g. Huyghe et al., 2001) and in the Bengal fan (Galy et al., 2010), the locus of rapid exhumation may have changed over time. Therefore, continuous rapid exhumation evidenced in the Bengal fan AFT data most likely reflects the underlying tectonic scheme driven by a permanent convergence between Asia and India and strong resulting uplift localized in limited areas such as the syntaxes or the hanging walls of crustal ramps.

7. Conclusions

Detrital AFT ages determined from turbidite deposits of the middle part of the Bengal fan provide a long-term record of Himalayan exhumation. Since at least 13 Ma, apatite grains with short minimum and central lag times (respectively 1.55±3.13 Myr and 2.26±1.6 Myr) were deposited in the Bengal fan. Apatite with such short lag times are also found in river sediments of the modern Ganges and Brahmaputra drainage system. Therefore, the lag time over the past 13 Ma and the modern lag time both support that temporary storage of detrital

497 apatite in the floodplains of the river drainage or in the delta are negligible and that
498 exhumation rates have been consistently fast on the order of at least 1-3 km/Myr. Therefore,
499 there have always been areas of fast erosion in the Himalayan range. Comparison of the AFT
500 data of the Bengal Fan with those of the Central and Eastern proximal Neogene Himalayan
501 foreland basin shows that both paleo Ganga and Brahmaputra catchments provided apatite
502 with short lag time to the distal Bengal fan basin. Additional provenance analysis is needed to
503 determine how such a fast exhumation varied in space and time.

504 The AFT data from the modern Himalayan erosion system show that apatites with
505 short AFT lag times are derived from zones undergoing relatively rapid exhumation along the
506 southern flank of the Himalaya. In these zones, the dominant processes of erosion are
507 controlled by high stream power of the rivers that efficiently transport fluvial sediments and
508 by a threshold angle triggering landslides and limiting the slope of the hills. Therefore, by
509 analogy with the modern erosion processes in the Himalayan range, we suggest that over the
510 past 13 Ma apatite were mainly derived from areas of sharp relief, where river stream power
511 was high and hill slopes close to the threshold angle. Consequently, the maximum exhumation
512 rate provided by the Bengal fan apatite were not strongly affected by climatic variations
513 related by the onset of the Plio-Pleistocene Northern Hemisphere cooling or by the reported
514 intensity changes of the Indian Monsoon. The maximum exhumation rates provided by the
515 minimum and central ages of the AFT of the Bengal fan are characteristic of the tectonic
516 processes at the Ma scale resolution.

517

518

519 **Acknowledgments**

520 This work was supported by IODP France and Labex Osug@2020 grants and the CNRS. We
521 thank Melanie Balvay, Francis Coeur and Francois Senebier of the Geo-Thermochronology
522 (GTC) platform at ISTerre, Université Grenoble Alpes, for help with sample preparation for
523 apatite fission-track analysis. The manuscript benefited from thorough and constructive
524 comments by P. Copeland, R. Thiede and A.A.G. Webb. We also thank D. Burbank and P.
525 DeCelles for improving an earlier version of the manuscript.

526

527 **References**
528

529 Abrahami, R., van der Beek, P., Huyghe, P., Hardwick, E., and Carcaillet, J., 2016. Decoupling of long-
530 term exhumation and short-term erosion rates in the Sikkim Himalaya, Earth and Planetary
531 Science Letters, 433, 76-88, 10.1016/j.epsl.2015.10.039.

532 Bernet, M., van der Beek, P., Pik, R., Huyghe, P., Mugnier, J.-L., Labrin, E., Szulc, A., 2006. Miocene
533 to Recent exhumation of the central Himalaya determined from combined detrital zircon fission-
534 track and U/Pb analysis of Siwalik sediments, western Nepal. Basin Research 18, 393-412,
535 https://doi.org/10.1111/j.1365-2117.2006.00303.x

536 Blythe, A.E., Burbank, D.W., Carter, A., Schmidt, K., Putkonen, J., 2007. Plio-Quaternary exhumation
537 history of the central Nepalese Himalaya: 1. Apatite and zircon fission track and apatite [U-
538 Th]/He analyses. Tectonics 26, n/a-n/a, https://doi.org/10.1029/2006tc001990

539 Bollinger, L., Henry, P., Avouac, J., 2006. Mountain building in the Nepal Himalaya: Thermal and
540 kinematic model. Earth and Planetary Science Letters 244, 58-71,
541 https://doi.org/10.1016/j.epsl.2006.01.045

542 Bookhagen, B., Burbank, D.W. 2010. Toward a complete Himalayan hydrological budget:
543 spatiotemporal distribution of snowmelt and rainfall and their impact on river discharge. J.
544 Geophys. Res. Earth Surf. 115:F03019. doi:10.1029 /2009JF001426.

Burbank, D.W., Blythe, A.E., Putkonen, J., Pratt-Sitaula, B., Gabet, E., Oskin, M., Barros, A., Ojha, T.P., 2003. Decoupling of erosion and precipitation in the Himalayas. Nature 426, 652-655, https://doi.org/10.1038/nature02187

Cerveny, P.F., Naeser, N.D., Zeitler, P.K., Naeser, C.W., Johnson, N.M., 1988. History of Uplift and Relief of the Himalaya During the Past 18 Million Years: Evidence from Fission-Track Ages of Detrital Zircons from Sandstones of the Siwalik Group, in: Kleinspehn, K.L., Paola, C. (Eds.), New Perspectives in Basin Analysis. Springer New York, New York, NY, pp. 43-61.

Chalaron, E., Mugnier, J.L., Mascle, G., 1995. Control on thrust tectonics in the Himalayan foothills: a view from a numerical model. Tectonophysics 248, 139-163, https://doi.org/10.1016/0040-1951(94)00281-d

Chirouze, F., Huyghe, P., van der Beek, P., Chauvel, C., Chakraborty, T., Dupont-Nivet, G., Bernet, M., 2013. Tectonics, exhumation, and drainage evolution of the eastern Himalaya since 13 Ma from detrital geochemistry and thermochronology, Kameng River Section, Arunachal Pradesh. Geological Society of America Bulletin 125, 523-538, https://doi.org/10.1130/b30697.1

Clift, P.D., Hodges, K.V., Heslop, D., Hannigan, R., Van Long, H., Calves, G., 2008. Correlation of Himalayan exhumation rates and Asian monsoon intensity. Nature Geoscience 1, 875-880, https://doi.org/10.1038/ngeo351

Copeland, P., and Harrison, T.M., 1990. Episodic rapid uplift in the Himalaya revealed by 40Ar/39AR analysis of detrital K-feldspar and muscovite, Bengal fan, Geology,, 18, 354-357, 10.1130/0091-7613(1990)018<0354:eruith>2.3.co;2

Corrigan, J.D., Crowley, K., 1990. Fission-Track Analysis of Detrital Apatites from Sites 717 and 718, Leg 116, Central Indian Ocean.

Coutand, I., Barrier, L., Govin, G., Grujic, D., Hoorn, C., Dupont-Nivet, G. and Najman, Y. 2016. Late Miocene- Pleistocene evolution of India-Eurasia convergence partitioning between the Bhutan Himalaya and the hillong Plateau: New evidences from foreland basin deposits along the Dungsam Chu section, eastern Bhutan, Tectonics, 35, 2963-2994, 10.1002/2016tc004258

571 DeCelles, P.G., Robinson, D.M., Quade, J., Ojha, T.P., Garzione, C.N., Copeland, P., Upreti, B.N.,
572 2001. Stratigraphy, structure, and tectonic evolution of the Himalayan fold-thrust belt in western
573 Nepal. Tectonics 20, 487-509, 10.1029/2000tc001226

574 Dettman, D.L., Kohn, M.J., Quade, J., Ryerson, F.J., Ojha, T.P., Hamidullah, S., 2001. Seasonal stable
575 isotope evidence for a strong Asian monsoon throughout the past 10.7 m.y. Geology 29, 31-34,
576 https://doi.org/10.1130/0091-7613(2001)029%3C0031:SSIEFA%3E2.0.CO;2

577 Elliott, J.R., Jolivet, R., González, P.J., Avouac, J.P., Hollingsworth, J., Searle, M.P., Stevens, V.L.,
578 2016. Himalayan megathrust geometry and relation to topography revealed by the Gorkha
579 earthquake. Nature Geoscience 9, 174-180, https://doi.org/10.1038/ngeo2623

580 France-Lanord, C., Spiess, V., Klaus, A., Schwenk, T., Scientists, t.E., 2016. Bengal Fan, in: France-
581 Lanord, C., Spiess, V., Klaus, A., Schwenk, T. (Eds.), Proceedings of the International Ocean
582 Discovery Program. International Ocean Discovery Program, College Station, TX.

583 Galbraith, R.F., 2005. Statistics for Fission Track Analysis. CRC Press, p. -219.

584 Galy, A., France-Lanord, C., Derry, L.A., 1996. The Late Oligocene-Early Miocene Himalayan belt
585 Constraints deduced from isotopic compositions of Early Miocene turbidites in the Bengal Fan.
586 Tectonophysics 260, 109-118, https://doi.org/10.1016/0040-1951(96)00079-0

587 Galy, V., France-Lanord, C., Peucker-Ehrenbrink, B., Huyghe, P., 2010. Sr–Nd–Os evidence for a
588 stable erosion regime in the Himalaya during the past 12Myr. Earth and Planetary Science
589 Letters 290, 474-480, https://doi.org/10.1016/j.epsl.2010.01.004

590 Garzanti, E., Andò, S., France-Lanord, C., Vezzoli, G., Censi, P., Galy, V., Najman, Y., 2010.
591 Mineralogical and chemical variability of fluvial sediments1. Bedload sand (Ganga–
592 Brahmaputra, Bangladesh). Earth and Planetary Science Letters 299, 368-381,
593 10.1016/j.epsl.2010.09.017

594 Gemignani, L., van der Beek, P., Braun, J., Naman, Y., Bernet, M., Garzanti, E. and Wijbrans, J.R.,
595 2018. Downstream evolution of the thermochronologic age signal in the Brahmaputra catchment

(eastern Himalaya): Implications for the detrital record of erosion. Earth and Planetary Science Letters 499, 48-61, doi.org/10.1016/j.epsl.2018.07.019

Godin, L., Grujic, D., Law, R.D., Searle, M.P., 2006. Channel flow, ductile extrusion and exhumation in continental collision zones: an introduction. Geological Society, London, Special Publications 268, 1,

Hasterok, D., Chapman, D.S., and Davis, E.E., 2011. Oceanic heat flow: impli- cations for global heat loss. Earth and Planetary Science Letters, 311(3– 4):386–395. http://dx.doi.org/10.1016/j.epsl.2011.09.044

Herman, F. , Seward, D., Valla, P.G., Carter, A., Kohn, B., Willett, S.D. and Ehlers, T.A., 2013. Worldwide acceleration of mountain erosion under a cooling climate, Nature, 504, 423-426, 10.1038/nataure12877.

Hodges, K.V., Wobus, C., Ruhl, K., Schildgen, T., Whipple, K., 2004. Quaternary deformation, river steepening, and heavy precipitation at the front of the Higher Himalayan ranges. Earth and Planetary Science Letters 220, 379-389, 10.1016/s0012-821x(04)00063-9

Hu, X., Garzanti, E., Moore, T. and Raffi, I, 2015. Direct stratigraphic dating of India-Asia collision onset at the Selandian (middle Paleocene, 59 ± 1 Ma, Geology, 43, 859-862, 10.1130/g36872.1.

Huyghe, P., Galy, A., Mugnier, J.-L., France-Lanord, C., 2001. Propagation of the thrust system and erosion in the Lesser Himalaya: Geochemical and sedimentological evidence. Geology 29, 1007-1010, https://doi.org/10.1130/0091-7613(2001)029%3C1007:POTTSA%3E2.0.CO;2

Krishna, K. S., M. Ismaiel, M., Srinivas, K., Gopala Rao, D., Mishra, J. and Saha, D., 2016. Sediment pathways and emergence of Himalayan source material in the Bay of Bengal Current Science, 110, 3, 363-372, doi: 10.18520/cs/v110/i3/363-372.

Lague, D., 2013. The stream power river incision model: evidence, theory and beyond. Earth Surface Processes and Landforms 39, 38-61, https://doi.org/10.1002/esp.3462

620 Larsen, I.J., Montgomery, D.R., 2012. Landslide erosion coupled to tectonics and river incision. Nature
621 Geoscience 5, 468, https://doi.org/10.1038/ngeo1479

622 Lavé, J., Avouac, J.P., 2001. Fluvial incision and tectonic uplift across the Himalayas of central Nepal.
623 Journal of Geophysical Research: Solid Earth 106, 26561-26591,
624 https://doi.org/10.1029/2001jb000359

625 Lupker, M., Lavé, J., France-Lanord, C., Christl, M., Bourlès, D., Carcaillet, J., Maden, C., Wieler, R.,
626 Rahman, M., Bezbaruah, D., Xiaohan, L., 2017. ^{10}Be systematics in the Tsangpo-Brahmaputra
627 catchment: the cosmogenic nuclide legacy of the eastern Himalayan syntaxis. Earth Surface
628 Dynamics 5, 429-449, 10.5194/esurf-5-429-2017

629 Mugnier, J.-L., and Huyghe, P., 2006. Ganges basin geometry records a pre-15 Ma isostatic rebound of
630 Himalaya. Geology 34, https://doi.org/10.1130/g22089.1

631 Najman, Y., Bickle, M., BouDagher-Fadel, M., Carter, A., Garzanti, E., Paul, M., Wijbrans, J., Willett,
632 E., Oliver, G., Parrish, R., Akhter, S.H., Allen, R., Ando, S., Chisty, E., Reisberg, L., Vezzoli, G.,
633 2008. The Paleogene record of Himalayan erosion: Bengal Basin, Bangladesh. Earth and
634 Planetary Science Letters 273, 1-14, https://doi.org/10.1016/j.epsl.2008.04.028

635 Reiners, P.W., Brandon, M.T., 2006. USING THERMOCHRONOLOGY TO UNDERSTAND
636 OROGENIC EROSION. Annual Review of Earth and Planetary Sciences 34, 419-466,
637 10.1146/annurev.earth.34.031405.125202

638 Reilly, B.T., 2018, Deciphering Quaternary geomagnetic, glacial, and depositional histories using
639 paleomagnetism in tandem with other chronostratigraphic and sedimentological approaches,
640 Ph.D. Thesis, Oregon State University, Corvallis, OR, 97331, USA

641 Robert, X., van der Beek, P., Braun, J., Perry, C., Mugnier, J.-L., 2011. Control of detachment geometry
642 on lateral variations in exhumation rates in the Himalaya: Insights from low-temperature
643 thermochronology and numerical modeling. Journal of Geophysical Research 116,
644 https://doi.org/10.1029/2010jb007893

Schildgen, T.F., van der Beek, P.A., Sinclair, H.D. and Thiede, R.C., 2018. Spacial correlation bias in late-Cenozoic erosion history derived from thermochronology, Nature, 559, 89-93, doi. org/10.1038/s41586-018-0260-6

Seward, D., and Burg, J.-P., 2008. Growth of the Namche Barwa Syntaxis and associated evolution of the Tsangpo Gorge: Constraints from structural and thermochronological data. Tectonophysics 451, 282-289, https://doi.org/10.1016/j.tecto.2007.11.057

Szulc, A.G., Najman, Y., Sinclair, H.D., Pringle, M., Bickle, M., Chapman, H., Garzanti, E., Andò, S., Huyghe, P., Mugnier, J.L., Ojha, T., DeCelles, P., 2006. Tectonic evolution of the Himalaya constrained by detrital 40Ar-39Ar, Sm-Nd and petrographic data from the Siwalik foreland basin succession, SW Nepal. Basin Research 18, 375-391, 10.1111/j.1365-2117.2006.00307.x

Thiede, R.C., Ehlers, T.A., 2013. Large spatial and temporal variations in Himalayan denudation. Earth and Planetary Science Letters 371-372, 278-293, https://doi.org/10.1016/j.epsl.2013.03.004

Tsou, C.-Y., Chigira, M., Higaki, D., Sato, G., Yagi, H., Sato, H.P., Wakai, A., Dangol, V., Amatya, S.C., Yatagai, A., 2018. Topographic and geologic controls on landslides induced by the 2015 Gorkha earthquake and its aftershocks: an example from the Trishuli Valley, central Nepal. Landslides 15, 953-965,

van der Beek, P., Robert, X., Mugnier, J.-L., Bernet, M., Huyghe, P., Labrin, E., 2006. Late Miocene – Recent exhumation of the central Himalaya and recycling in the foreland basin assessed by apatite fission-track thermochronology of Siwalik sediments, Nepal. Basin Research 18, 413-434, https://doi.org/10.1111/j.1365-2117.2006.00305.x

Vermeesch, P., 2009, RadialPlotter: A Java application for fission track, luminescence and other radial plots. Radiation Measurements, 44, 409-410.

Webb, A.A.G, Guo, H., Clift, P.D., Husson, L., Müller, T., Costantino, D., Yin, A., Xu, Z., Cao, H., and Wang, Q., 2017, The Himalaya in 3D: Slab dynamics controlled mountain building and monsoon intensification, Lithosphere, 9, 637–651. doi: https://doi.org/10.1130/L636.1

Whipple, K.X., Shirzaei, M., Hodges, K.V., Ramon Arrowsmith, J., 2016. Active shortening within the Himalayan orogenic wedge implied by the 2015 Gorkha earthquake. Nature Geoscience 9, 711, https://doi.org/10.1038/ngeo2797

Whipple, K.X., Tucker, G.E., 2002. Implications of sediment-flux-dependent river incision models for landscape evolution. Journal of Geophysical Research: Solid Earth 107, ETG 3-1-ETG 3-20, 10.1029/2000JB000044

Yin, A., Harrison, T.M., Murphy, M.A., Grove, M., Nie, S., Ryerson, F.J., Feng, W.X., Le, C.Z., 1999. Tertiary deformation history of southeastern and southwestern Tibet during the Indo-Asian collision. Geological Society of America Bulletin 111, 1644– 1664, https://doi.org/10.1130/0016-7606.

Zeitler, P.K., Koons, P.O., Bishop, M.P., Chamberlain, C.P., Craw, D., Edwards, M.A., Hamidullah, S., Jan, M.Q., Khan, M.A., Khattak, M.U.K., Kidd, W.S.F., Mackie, R.L., Meltzer, A.S., Park, S.K., Pecher, A., Poage, M.A., Sarker, G., Schneider, D.A., Seeber, L., Shroder, J.F., 2001. Crustal reworking at Nanga Parbat, Pakistan: Metamorphic consequences of thermal-mechanical coupling facilitated by erosion. Tectonics 20, 712-728, https://doi.org/10.1029/2000tc001243

Figure captions

Figure 1:

A) The Ganga-Brahmaputra catchment of the Bengal Fan (from Galy et al. 2010) - B: Bhopal; C: Kolkata; D: Delhi; K: Kathmandu; NBS: Namche Barwa Syntaxis; THB: Tran-Himalayan Batholiths. River names are those cited in the text and are indicated by the following symbols. α: SunKoshi, β: Brahmaputra; χ: Subansiri; δ: Rangit, ε: Kameng, ϕ: Marsyandi and Daraundi, γ: Bhote Kosi, λ: Karnali; η: Siang; μ: Dibang; ρ: Rapti.Location of sampling is displayed by stars for apatites.

B): Sketch of the inferred structural elements of the Indo-Asia collision zone controlling localized rapid exhumation rates (orange, purple and red lines refer respectively to the 110°C isotherm related to the AFT closure temperature, to the brittle/ductile transition and to the 750°C isotherm below which partial melt starts). In the brittle regime : 1) the Main Himalayan Thrust (MHT) is affected by a crustal ramp (e.g. Elliot et al., 2016) that migrated during the evolution of the range and delineates duplexes (e.g. De Celles et al., 1998); 2) internal shortening (Whipple et al., 2016) including 3) out-of-sequence thrust (Hodges et al., 2004); In the ductile regime (thin lines): distributed shearing (horizontal arrows) and vertical flattening define a channel flow (ChF) (Godin et al., 2013) with a fast exhumation zone (4) at its frontal edge and/or (5) a lateral extrusion in the syntaxes (e.g. Zeitler et al., 2001).

Figure 2: Variation of the AFT central ages (blue diamond) and AFT minimum ages (red square) versus depth for the two drilling sites U1450 and U1451 (Bengal Fan, 8°N). Horizontal bars correspond to 2σ uncertainty. Red line represents the age model based on the magnetostratigraphic model of Reilly (2018) for the <1.9 Ma deposits and on polynomial extrapolation between shipboard and post-cruise biostratigraphic constraints based on nannofossil zones (France Lanord et al., 2016). The minimum age curve (grey dotted line) is established from the youngest fauna considering that older fauna in turbidite horizons could be reworking by the turbiditic current.

Figure 3: A) Cumulative AFT age plots, organized from youngest to oldest grains of selected samples showing the 95% age confidence intervals. Samples U1450A 24HG and U1450A 110F with respectively 100 and less than 30 counted grains are shown for comparison of the robustness of AFT ages; B) Apatite fission-track age radial plots of corresponding Bengal fan samples, showing central and minimum ages determined with RadialPlotter (Vermeesch, 2009). Radial plots and cumulative age plots of all samples are available in the Appendix B.

722 Figure 4: Radial plots of samples U1450A 6 7 8F (minimum and AFT central ages older than
723 depositional age), U1451A 37F2 (minimum and AFT central ages younger than depositional
724 age) and U1451B 45R1 (minimum and AFT central ages that overlap with the 2-sigma error
725 range with its depositional age) are shown for comparison. Radial plot of sample U1451B
726 45R1, displays a trend of apatite with younger cooling ages and higher U concentrations.

727 Figure 5: A) Single grain AFT age versus U concentration plot of detrital apatite grains of
728 sample series U1450A and U1451A. B) Plot for apatite with fission-track cooling ages <2Ma).
729 C) Single grain AFT age versus U concentration plot of detrital apatite grains from modern
730 Himalayan river sediments. The red dotted line correspond(s) to 10 ppm U concentration
731 below which grains are considered to have a poor U content.

732 Figure 6: AFT age radial plots of the new Himalaya river samples presented in this study,
733 showing central and minimum ages determined with RadialPlotter (Vermeesch, 2009).

734 Figure 7: Comparison between Bengal Fan, Siwaliks and Himalayan rivers AFT central ages.
735 Bengal Fan AFT data are represented by blue diamonds, Siwalik AFT data from Central
736 Himalaya (Van der Beek et al., 2006) by squares and Siwalik AFT data from Eastern
737 Himalaya (Chirouze et al., 2013, Coutand et al., 2016) by triangles. Yellow squares and
738 triangles represent AFT central ages of Himalayan rivers belonging, respectively, to the Ganga
739 and Brahmaputra rivers.

740 Figure 8: Relationships between sharp topographic transition in Himalaya, exhumation short
741 AFT lag time and transport toward the proximal and distal Bengal Fan foreland basins. When
742 the 110°C exhumation path of apatite crystals (green line), reaches the topography, erosion
743 occurs and material containing apatite is shed to the river system (blue line and arrows) and
744 finally to the Bengal Fan. Green circles indicate the FT central lag time (in Myr) of detrital
745 apatites in the rivers running in the proximal foreland basin and in the Bengal fan distal basin;

green squares indicate the *in situ* age range of the apatite provided by the steepest slopes. Three sketches are drawn from the available AFT data: modern Himalaya, 6-7 Ma Himalaya, 12-13 Ma Himalaya.

A) sketch of the Bengal fan U1451 drill hole (from France-Lanord et al. 2016) recording short AFT lag times since 13 Ma. For caption of the drill hole lithology, see Figure 2.

B) modern Himalayan sketch with sharp topographic transition above the ramp system and in the Namche Barwa syntaxis (NB). Recent AFT of the Bengal Fan and AFT of Himalayan rivers are from this paper. *In situ* AFT ages are from Burbank et al. (2003) and Blythe et al. (2007) above the Himalayan ramp system. *In situ* AFT ages are from Seward and Burg (2008) for the Namche Barwa syntaxis.

C) sketch of the persistence of very steep mountain zones related to rapid exhumation zone in Himalaya from 6-7 Ma to the present-day, as suggested by the AFT of the < 6-7 Ma Siwalik and Bengal Fan sedimentary records (van der Beck et al., 2006; Chirouze et al., 2013; Coutand et al., 2016 and this study); D) sketch of the persistence of very steep mountain zones related to fast exhumation zone in Himalaya from 7 to 13 Ma (as suggested by the Bengal fan sedimentary record, this study). No indication is given for the paleo-Himalayan rivers as AFT of the Siwalik proximal basin are reset.

Tables

Table 1. Bengal fan detrital apatite fission-track data and central age lag-time estimates for samples from the IODP 345 sites 1450 and 1451

Table 2. Central and eastern Himalayan river detrital apatite fission-track data and sample locations

Supplementary material:

771 Appendix A: Details of composite samples of the Bengal Fan

772 Appendix B: Bengal fan data set - Apatite fission-track single grain age data, Apatite fission-
773 track radial plots and grain age 95% confidence interval plots

774 Appendix C: Himalayan rivers data set - Apatite fission-track single grain age data and Apatite
775 fission-track radial plots

776 Appendix D: Lag time to exhumation rate relationship determined with the 1D thermal
777 advection model Age2Edot of Brandon (see Ehlers et al. 2005) for F-apatites.

778

779

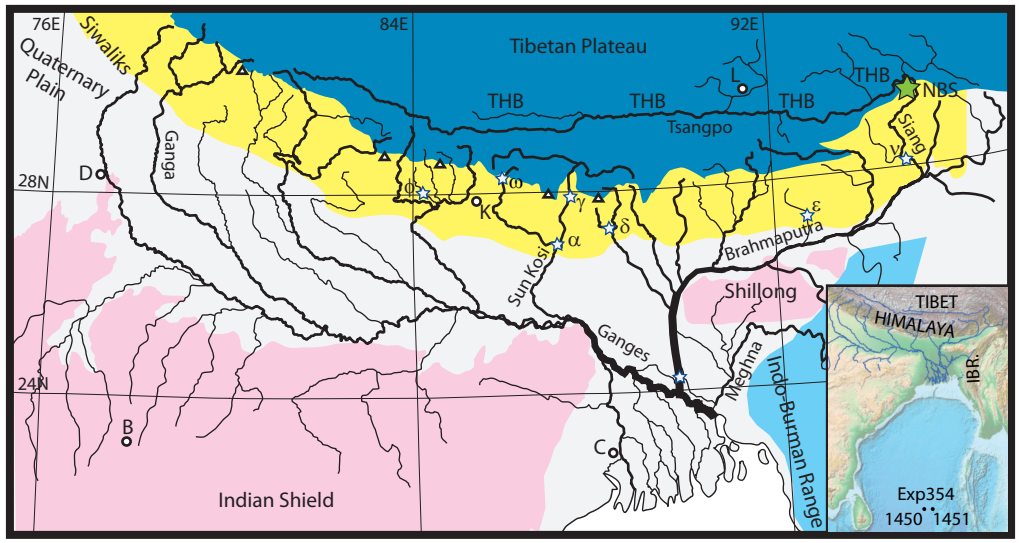

Figure 1a

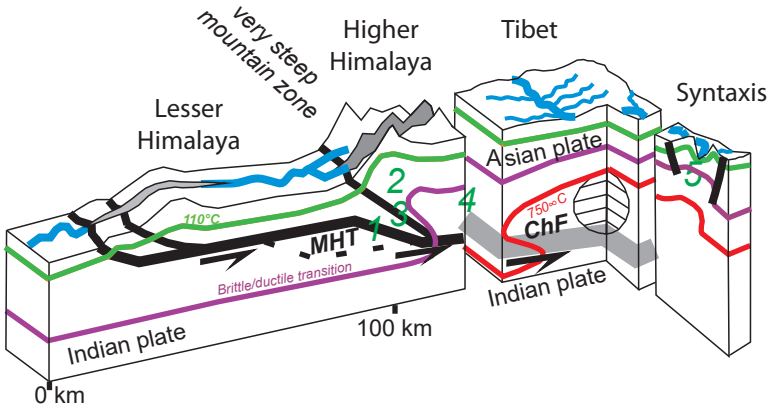

Figure 1b

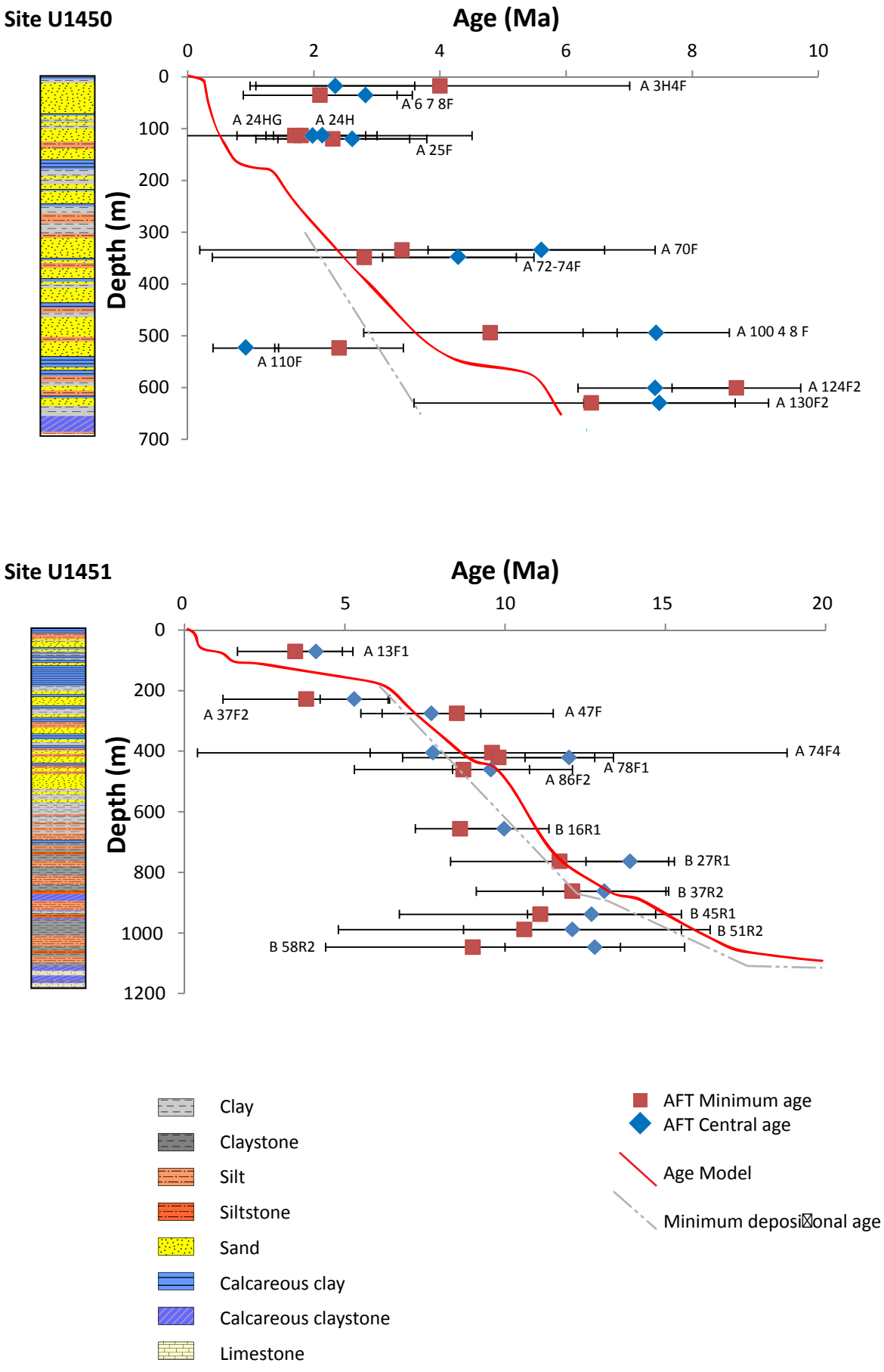
Site U1450
Age (Ma)
0
2
4
6
8
10
Depth (m)
0
100
200
300
400
500
600
700
A 3H4F
A 6 7 8F
A 24HG
A 24H
A 25F
A 70F
A 72-74F
A 100 4 8 F
A 110F
A 124F2
A 130F2
Site U1451
Age (Ma)
0
5
10
15
20
Depth (m)
0
200
400
600
800
1000
1200
A 13F1
A 37F2
A 47F
A 74F4
A 78F1
A 86F2
B 16R1
B 27R1
B 37R2
B 45R1
B 51R2
B 58R2
Clay
Claystone
Silt
Siltstone
Sand
Calcareous clay
Calcareous claystone
Limestone
AFT Minimum age
AFT Central age
Age Model
Minimum deposi⊠onal age

Figure 2

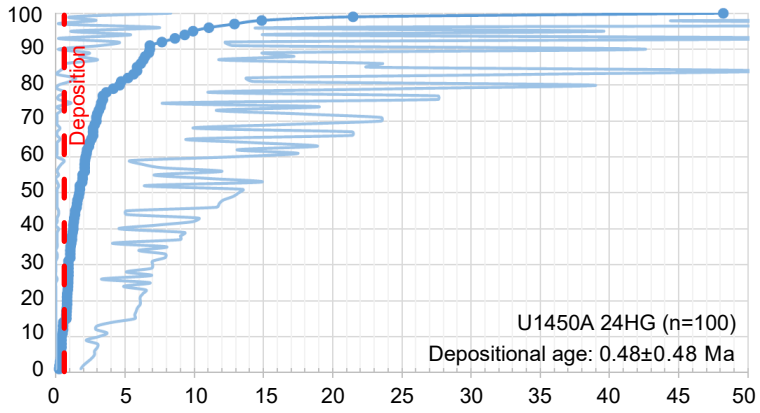
Deposition
U1450A 24HG (n=100)
Depositional age: 0.48±0.48 Ma

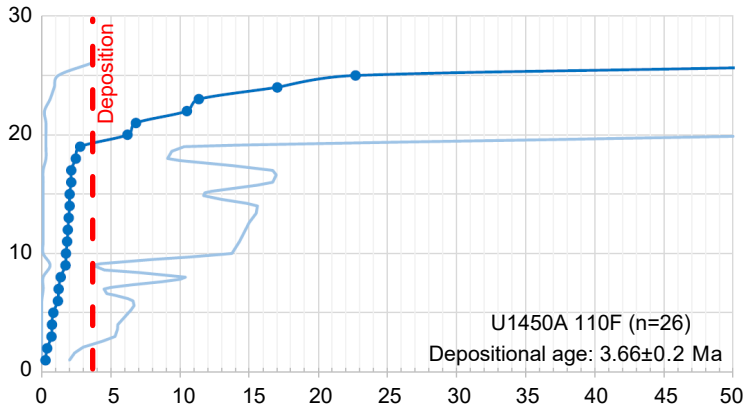
Deposition
U1450A 110F (n=26)
Depositional age: 3.66±0.2 Ma

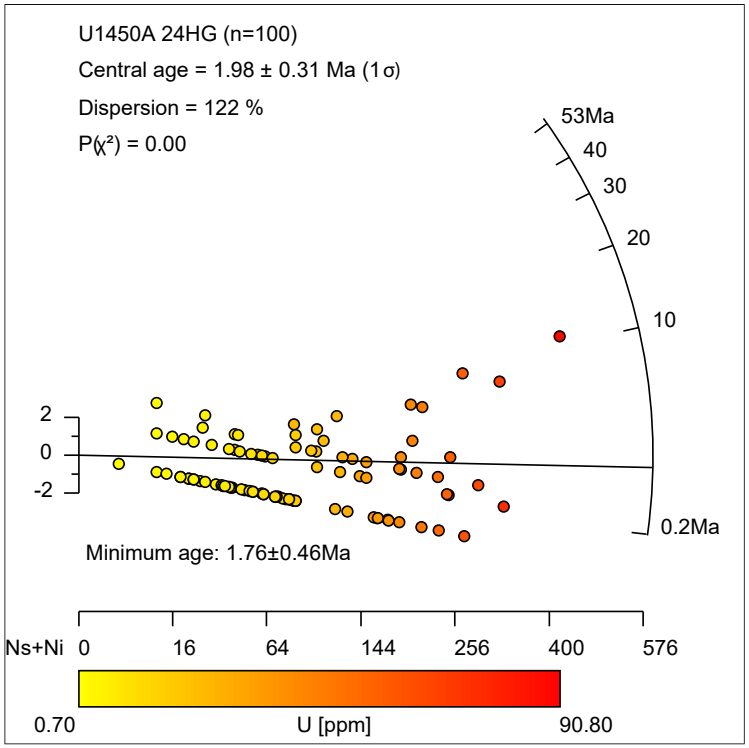
U1450A 24HG (n=100)
Central age = 1.98 ± 0.31 Ma (1σ)
Dispersion = 122 %
P(χ²) = 0.00
53Ma
0.2Ma
Minimum age: 1.76±0.46Ma
Ns+Ni
U [ppm]
0.70
90.80

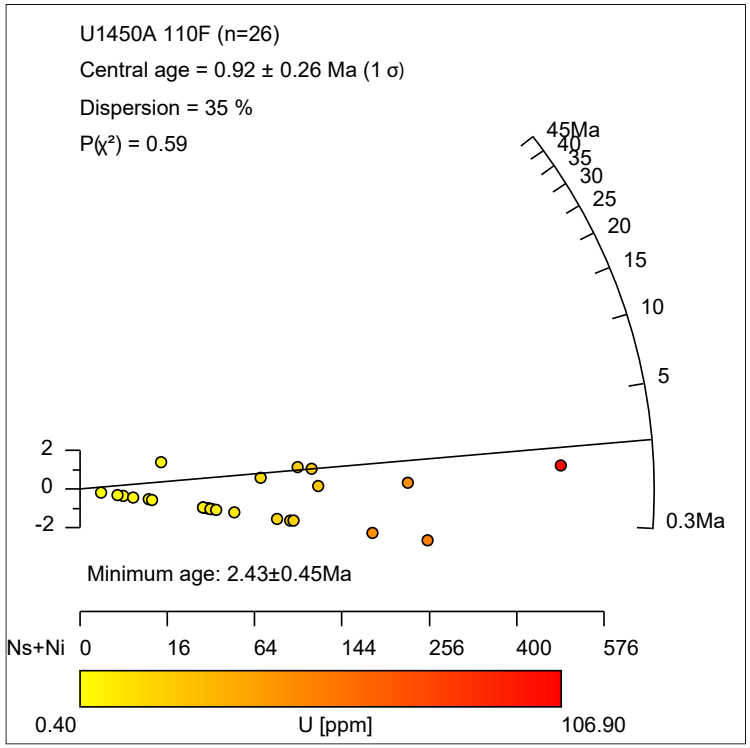
U1450A 110F (n=26)
Central age = 0.92 ± 0.26 Ma (1 σ)
Dispersion = 35 %
P(χ²) = 0.59
45Ma
0.3Ma
Minimum age: 2.43±0.45Ma
Ns+Ni
U [ppm]
0.40
106.90

Figure 3

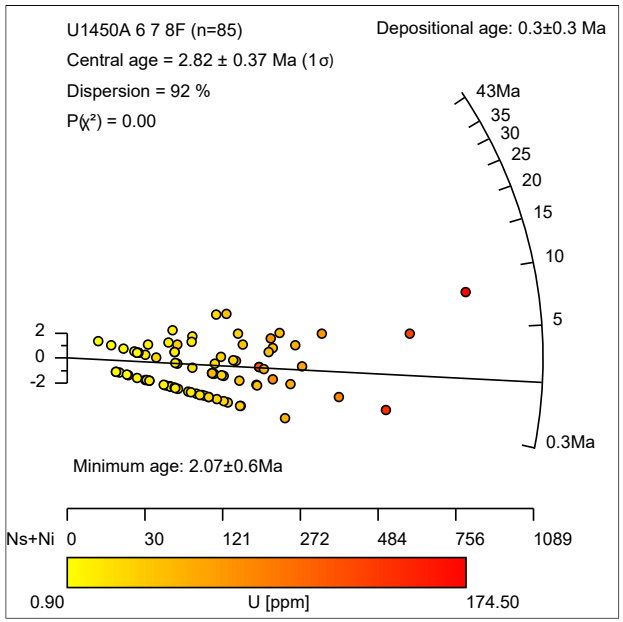
U1450A 6 7 8F (n=85)
Depositional age: 0.3±0.3 Ma
Central age = 2.82 ± 0.37 Ma (1σ)
Dispersion = 92 %
P(χ²) = 0.00
43Ma
35
30
25
20
15
10
5
0.3Ma
2
0
-2
Minimum age: 2.07±0.6Ma
Ns+Ni 0 30 121 272 484 756 1089
0.90 U [ppm] 174.50

(a)

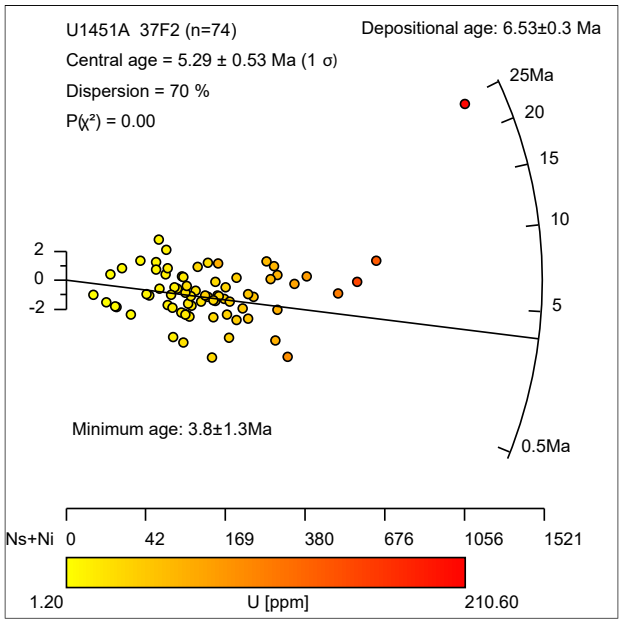
U1451A 37F2 (n=74)
Depositional age: 6.53±0.3 Ma
Central age = 5.29 ± 0.53 Ma (1 σ)
Dispersion = 70 %
P(χ²) = 0.00
25Ma
20
15
10
5
0.5Ma
2
0
-2
Minimum age: 3.8±1.3Ma
Ns+Ni 0 42 169 380 676 1056 1521
1.20 U [ppm] 210.60

(b)

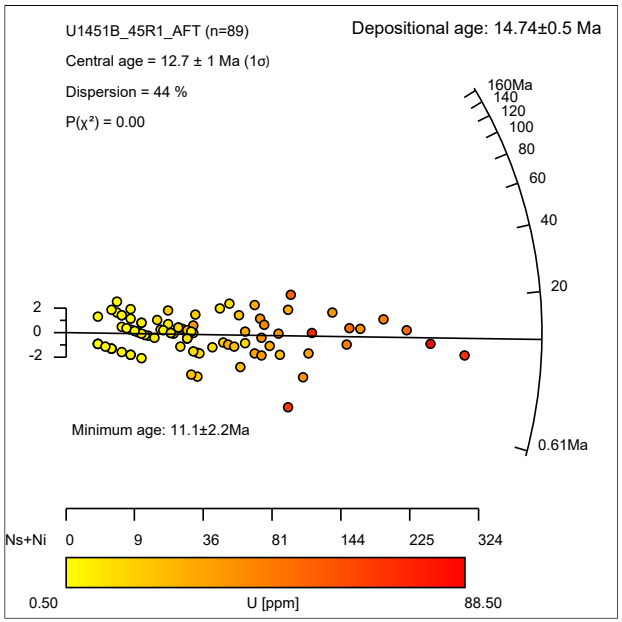
U1451B_45R1_AFT (n=89)
Depositional age: 14.74±0.5 Ma
Central age = 12.7 ± 1 Ma (1σ)
Dispersion = 44 %
P(χ²) = 0.00
160Ma
140
120
100
80
60
40
20
0.61Ma
2
0
-2
Minimum age: 11.1±2.2Ma
Ns+Ni 0 9 36 81 144 225 324
0.50 U [ppm] 88.50

(c)

Figure 4

A)

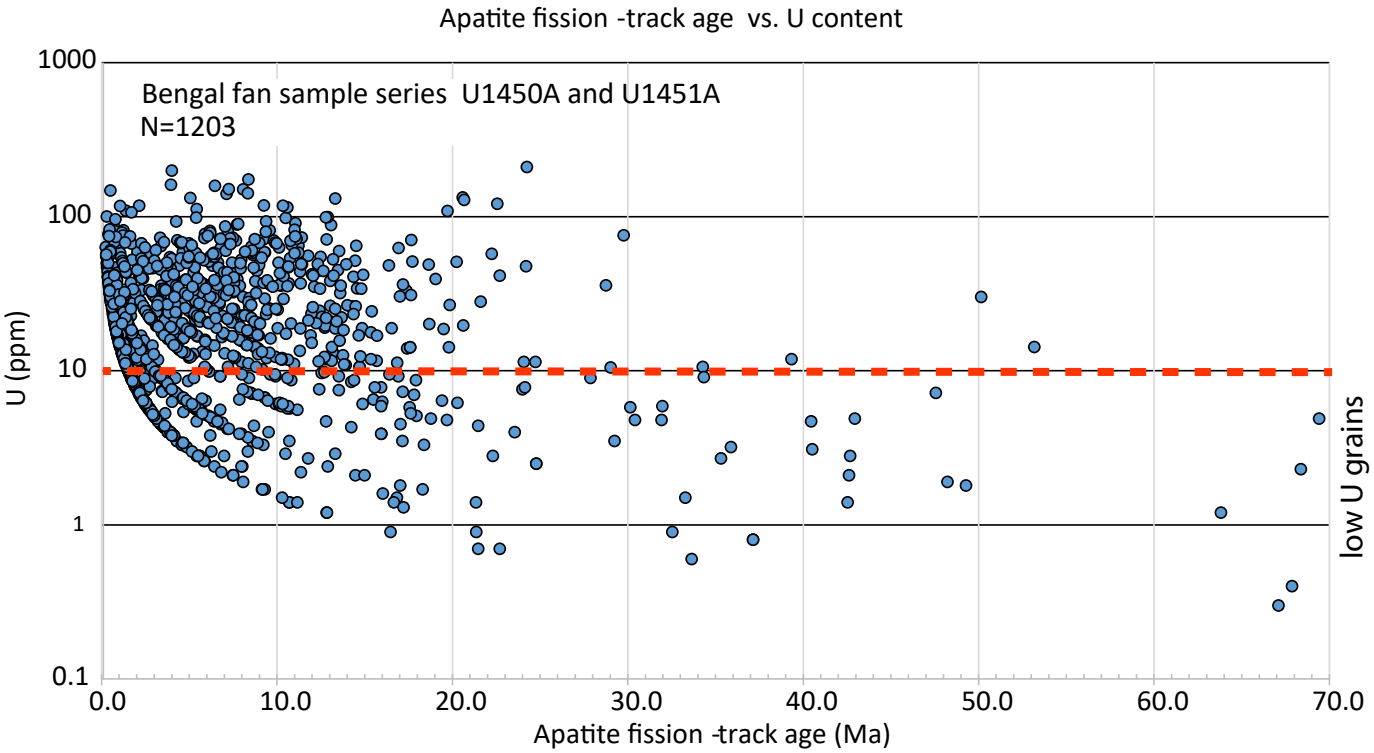
Apatite fission -track age vs. U content
Bengal fan sample series U1450A and U1451A
N=1203
U (ppm)
1000
100
10
1
0.1
0.0
10.0
20.0
30.0
40.0
50.0
60.0
70.0
Apatite fission -track age (Ma)
low U grains

B)

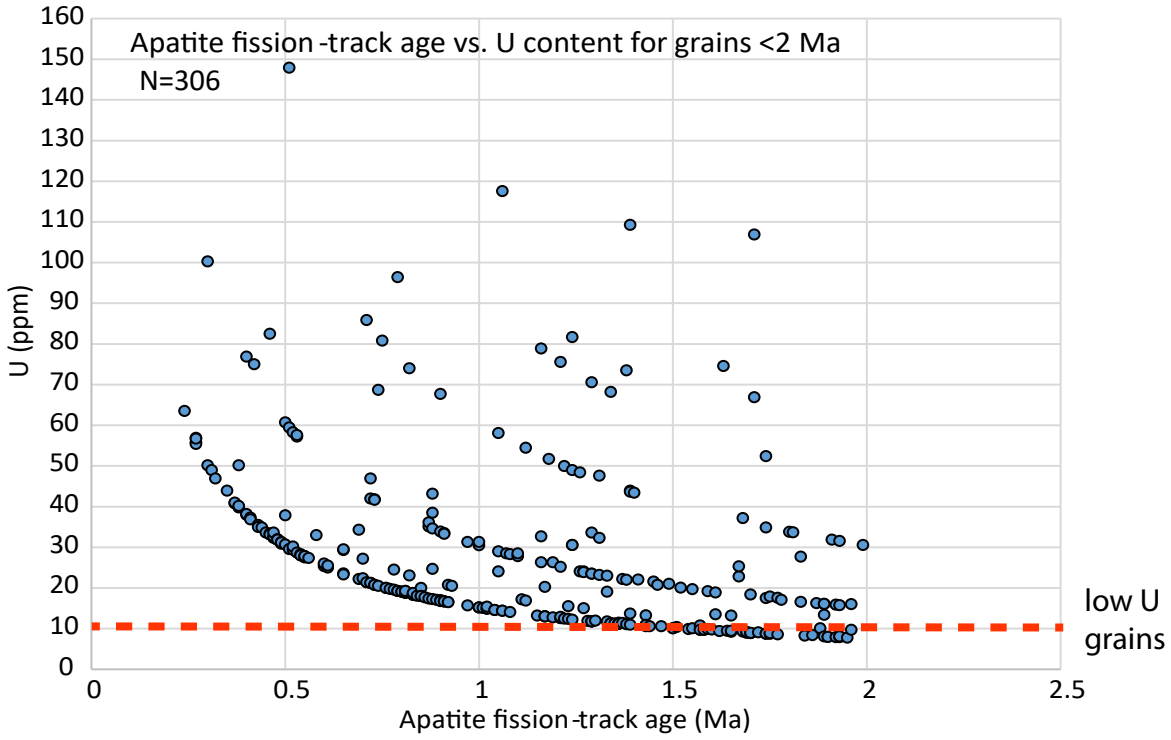
Apatite fission -track age vs. U content for grains <2 Ma
N=306
U (ppm)
160
150
140
130
120
110
100
90
80
70
60
50
40
30
20
10
0
0
0.5
1
1.5
2
2.5
Apatite fission -track age (Ma)
low U grains

C)

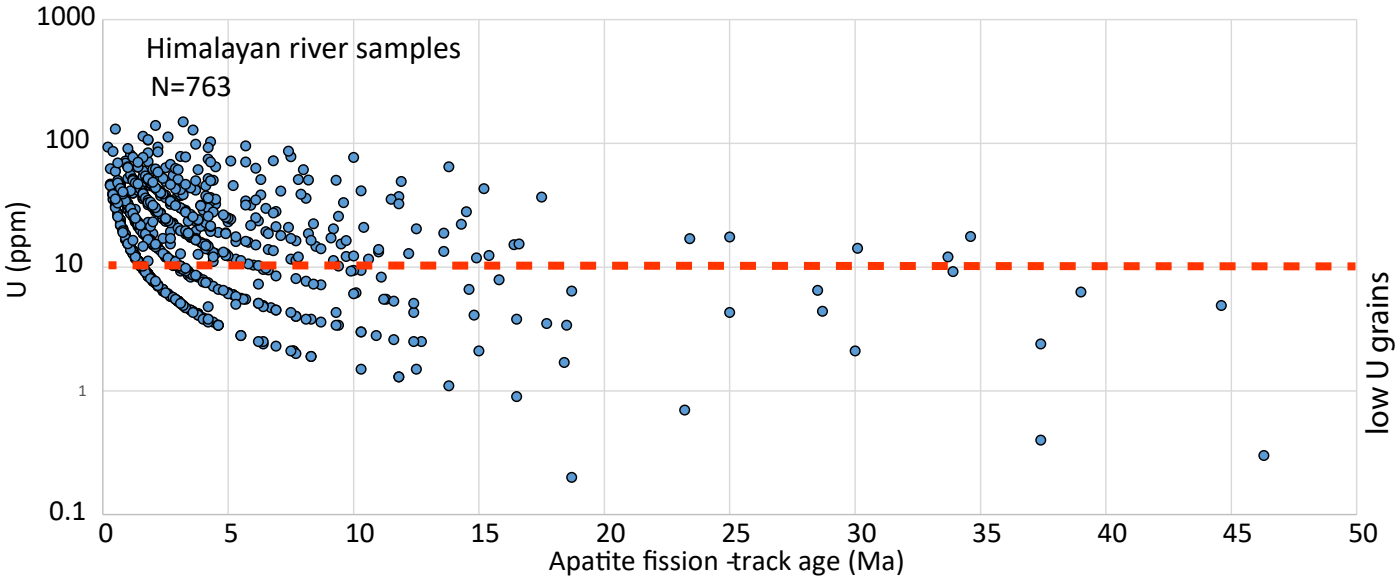
Himalayan river samples
N=763
U (ppm)
1000
100
10
1
0.1
0
5
10
15
20
25
30
35
40
45
50
Apatite fission -track age (Ma)
low U grains

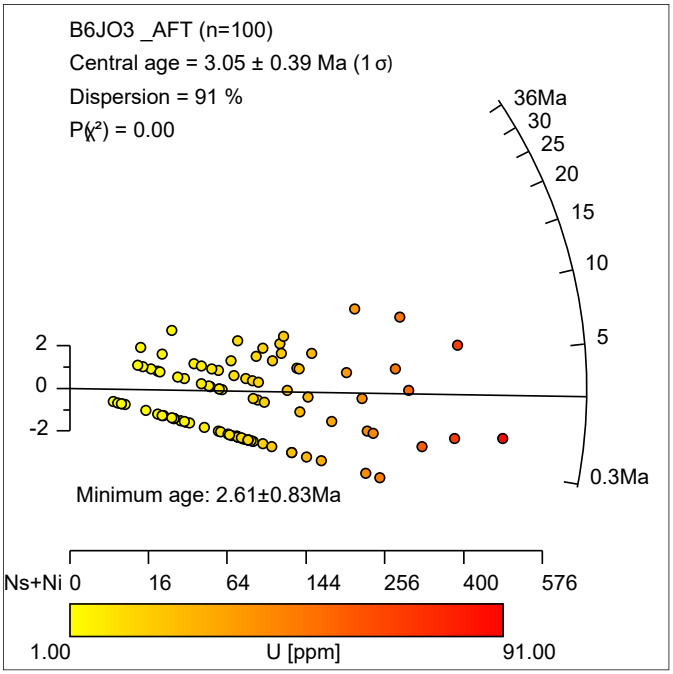
B6JO3 _AFT (n=100)
Central age = 3.05 ± 0.39 Ma (1 σ)
Dispersion = 91 %
P(χ²) = 0.00
36Ma
30
25
20
15
10
5
0.3Ma
2
0
-2
Minimum age: 2.61±0.83Ma
Ns+Ni 0 16 64 144 256 400 576
1.00 U [ppm] 91.00

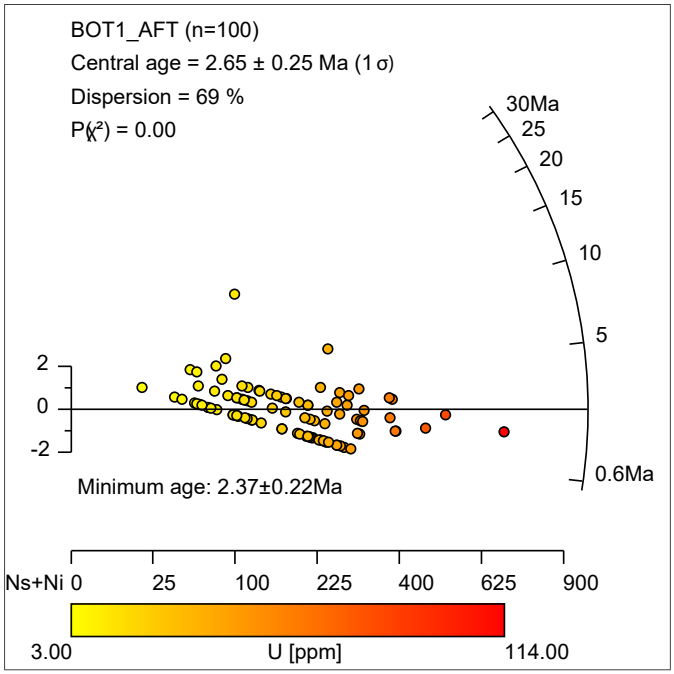
BOT1_AFT (n=100)
Central age = 2.65 ± 0.25 Ma (1 σ)
Dispersion = 69 %
P(χ²) = 0.00
30Ma
25
20
15
10
5
0.6Ma
2
0
-2
Minimum age: 2.37±0.22Ma
Ns+Ni 0 25 100 225 400 625 900
3.00 U [ppm] 114.00

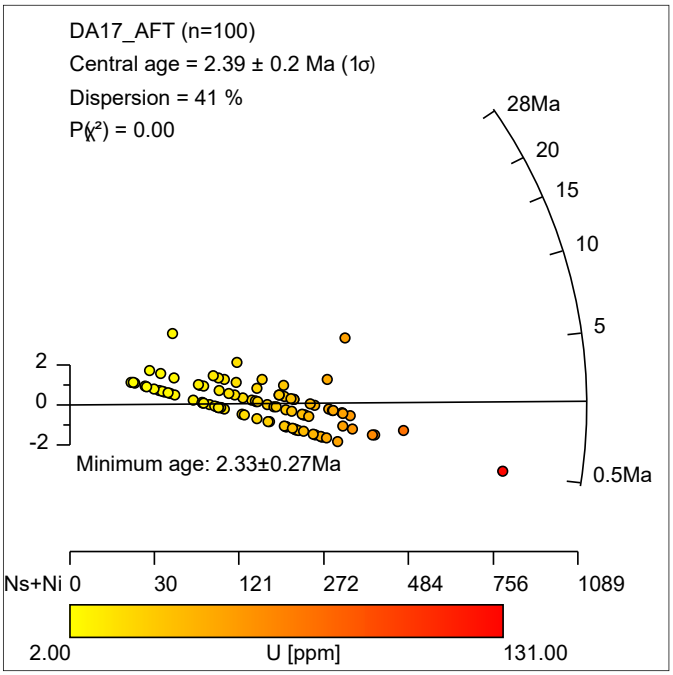
DA17_AFT (n=100)
Central age = 2.39 ± 0.2 Ma (1σ)
Dispersion = 41 %
P(χ²) = 0.00
28Ma
20
15
10
5
0.5Ma
2
0
-2
Minimum age: 2.33±0.27Ma
Ns+Ni 0 30 121 272 484 756 1089
2.00 U [ppm] 131.00

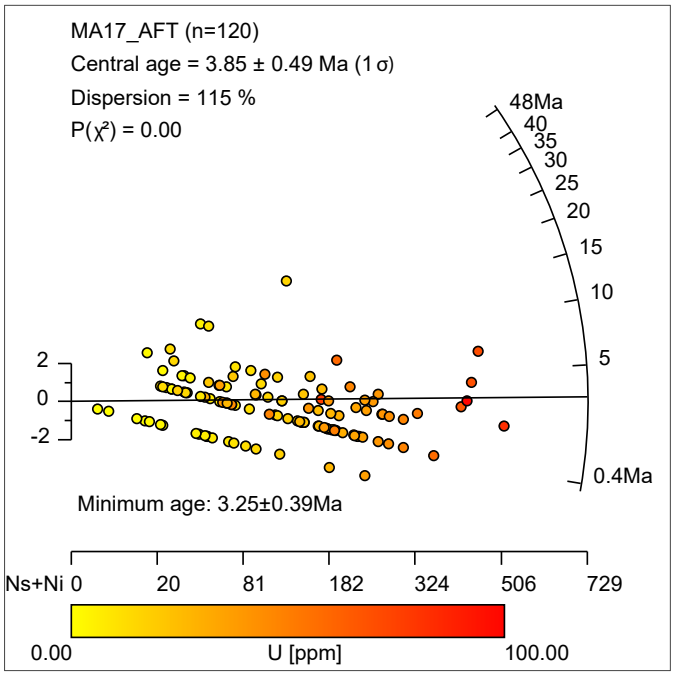
MA17_AFT (n=120)
Central age = 3.85 ± 0.49 Ma (1 σ)
Dispersion = 115 %
P(χ²) = 0.00
48Ma
40
35
30
25
20
15
10
5
0.4Ma
2
0
-2
Minimum age: 3.25±0.39Ma
Ns+Ni 0 20 81 182 324 506 729
0.00 U [ppm] 100.00

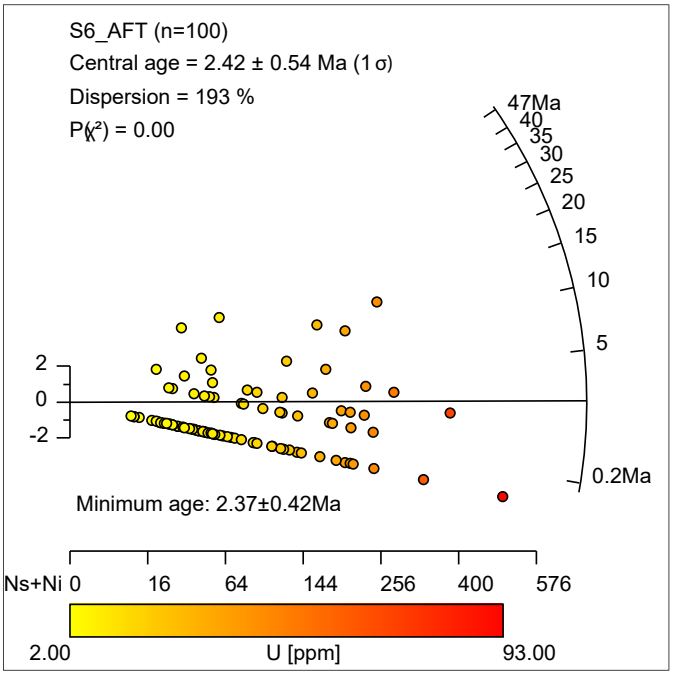
S6_AFT (n=100)
Central age = 2.42 ± 0.54 Ma (1 σ)
Dispersion = 193 %
P(χ²) = 0.00
47Ma
40
35
30
25
20
15
10
5
0.2Ma
2
0
-2
Minimum age: 2.37±0.42Ma
Ns+Ni 0 16 64 144 256 400 576
2.00 U [ppm] 93.00

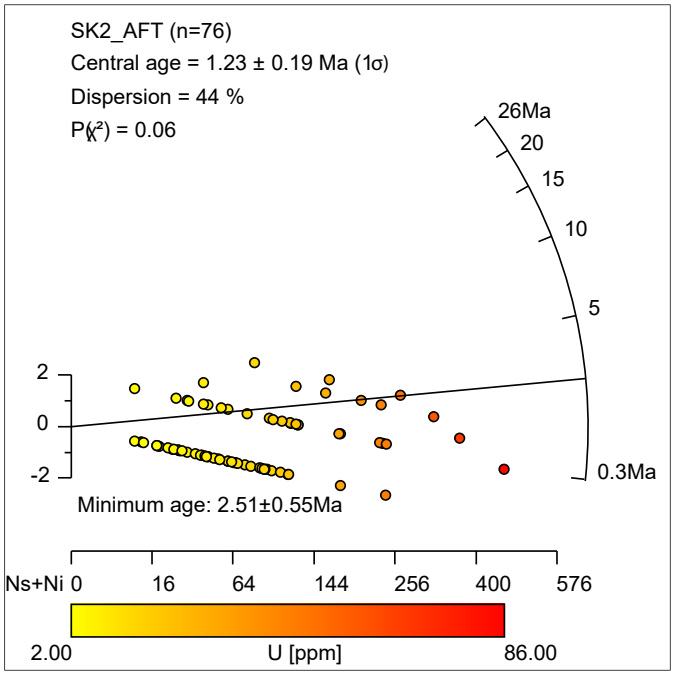
SK2_AFT (n=76)
Central age = 1.23 ± 0.19 Ma (1σ)
Dispersion = 44 %
P(χ²) = 0.06
26Ma
20
15
10
5
0.3Ma
2
0
-2
Minimum age: 2.51±0.55Ma
Ns+Ni 0 16 64 144 256 400 576
2.00 U [ppm] 86.00

Fig. 6

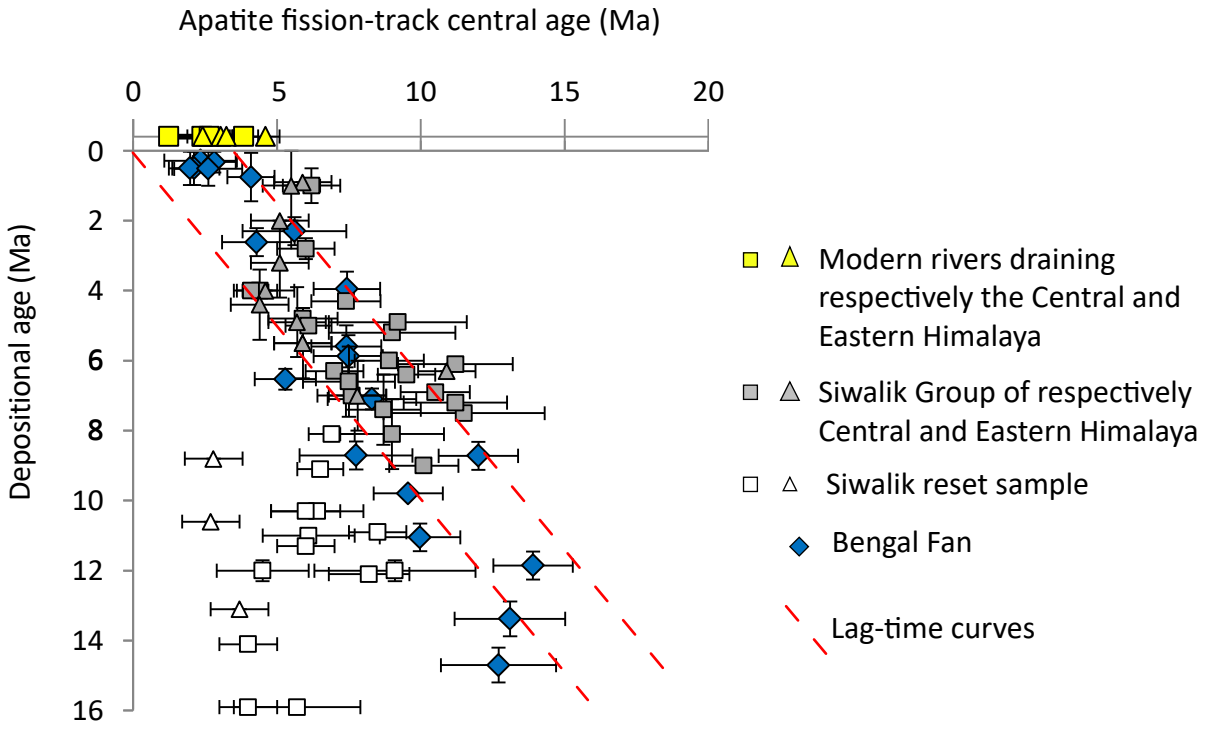
Apatite fission-track central age (Ma)
0
5
10
15
20
Depositional age (Ma)
0
2
4
6
8
10
12
14
16
Modern rivers draining respectively the Central and Eastern Himalaya
Siwalik Group of respectively Central and Eastern Himalaya
Siwalik reset sample
Bengal Fan
Lag-time curves

Figure 7

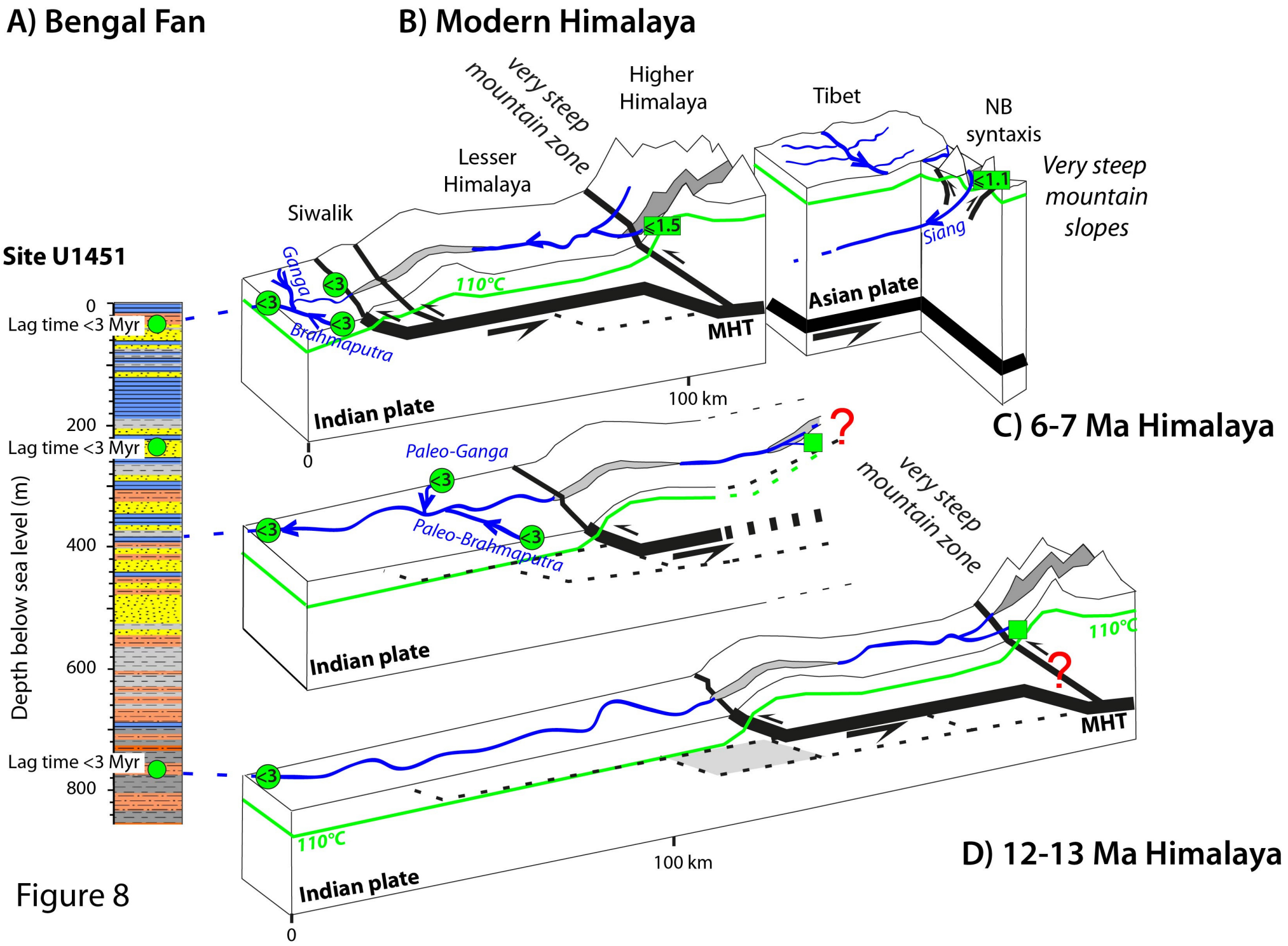
A) Bengal Fan
B) Modern Himalaya
Site U1451
Lag time <3 Myr
Lag time <3 Myr
Lag time <3 Myr
Depth below sea level (m)
0
200
400
600
800
very steep mountain zone
Higher Himalaya
Tibet
NB syntaxis
Lesser Himalaya
Siwalik
Very steep mountain slopes
≤1.5
≤1.1
Ganga
Brahmaputra
Siang
110°C
Asian plate
MHT
Indian plate
100 km
0
C) 6-7 Ma Himalaya
Paleo-Ganga
Paleo-Brahmaputra
very steep mountain zone
Indian plate
110°C
MHT
D) 12-13 Ma Himalaya
110°C
Indian plate
100 km
0

Figure 8